THE ANALYSIS OF NOISE VOLTAGE COUPLING BETWEEN RIGHT-HANDED AND META-MATERIALS INSPIRED TRANSMISSION LINES ON PRINTED CIRCUIT BOARDS

A Thesis
Submitted to the Graduate Faculty
of the
North Dakota State University
of Agriculture and Applied Science

By

Sanjay Nariyal

In Partial Fulfillment of the Requirements
for the Degree of
MASTER OF SCIENCE

Major Department:
Electrical and Computer Engineering

April 2013

Fargo, North Dakota

North Dakota State University
Graduate School

Title

THE ANALYSIS OF NOISE VOLTAGE COUPLING BETWEEN RIGHT-HANDED AND META-MATERIALS INSPIRED TRANSMISSION LINES ON PRINTED CIRCUIT BOARDS

By

Sanjay Nariyal

The Supervisory Committee certifies that this ***disquisition*** complies with North Dakota State University's regulations and meets the accepted standards for the degree of

MASTER OF SCIENCE

SUPERVISORY COMMITTEE:

Dr. Benjamin D. Braaten
Chair

Dr. David A. Rogers

Dr. Debasis Dawn

Dr. Alan Denton

Approved:

4/8/2013
Date

Dr. Rajendra Katti
Department Chair

ABSTRACT

An important consideration of RF circuitry in terms of Electromagnetic Compatibility is the correct modeling of the coupling between printed transmission lines. This is very important because the coupled noise voltages that are generated between two lines may cause adverse effects on sensitive components placed in the close vicinity. To study this problem of coupling in terms of noise voltages, first the analytical expressions for computing the near-end and far-end voltages between the conventional Right-Handed (RH) and Composite Right-/Left-Handed Transmission Lines (CRLH-TLs) and then RH and Complementary Split Ring Resonators (CSRR-TLs) were derived. The obtained expressions were then successfully validated with the simulation and measurements results. These expressions will give us an insight on how to reduce the induced noise voltages on the CRLH- and CSRR-TLs by varying the capacitance and inductance values that support left-handed propagation. In particular, it will be shown that the noise voltages coupled to the CRLH-TL are approximately 10 dB lower than the voltages coupled to the CSRR-TL. This could prove to be a useful alternative to conventional shielding.

ACKNOWLEDGMENTS

First, I would like to thank my advisor, Dr. Benjamin D. Braaten, for his great guidance, highly required encouragement and motivation, and the time spent by him in helping me get to this point and finish this work in time.

I would like to thank my committee members Dr. David Rogers, Dr. Alan Denton, and Dr. Debasis Dawn who also played a crucial role in helping me grasp the concepts which I went on to use in this work. I am very grateful for their support and participation.

I also would like to thank my colleagues for providing a competitive and learning environment that has encouraged me to strive for better and has enriched my experience.

DEDICATION

To my parents and in loving memory of my brother.

TABLE OF CONTENTS

LIST OF TABLES

LIST OF FIGURES

LIST OF SYMBOLS

n ..... Refractive Index of the Medium

ϵ_r ..... Relative Permittivity of the Medium

μ_r ..... Relative Permeability of the Medium

MTM ..... Meta-Material

TL ..... Transmission Line

RH ..... Right Handed

LH ..... Left Handed

$CRLH$ ..... Composite Right Left Handed

$CSRR$ ..... Composite Split Ring Resonator

TWs ..... Thin Wires

$SRRs$ ..... Split Ring Resonators

γ ..... Propagation Constant of the Medium

α ..... Attenuation Constant of the Medium

β ..... Phase Constant of the Medium

ω ..... Angular Frequency

ω_1 .. Minimum Angular Frequency of the Resonant Circuits in CRLH-TL for an Unbalanced Case

ω_2 .. Maximum Angular Frequency of the Resonant Circuits in CRLH-TL for an Unbalanced Case

ω_0 ..... Angular Frequency of Resonant Circuits in CRLH-TL for a Balanced Case.

$Z(\omega)$ ..... Impedance of the Series Branch in the Circuit

$Y(\omega)$ ..... Admittance of the Parallel Branch in the Circuit

Z_c ..... Characteristic Impedance of the TL

L_R ..... Right Handed Inductance

C_R ..... Right Handed Capacitance

L_L ..... Left Handed Inductance

C_L ..... Left Handed Capacitance

β_{RH-TL} ..... Phase Constant of the RH-TL

β_{LH-TL} ..... Phase Constant of the LH-TL

$Z_{c,RH-TL}$ ..... Characteristic Impedance of the RH-TL

$Z_{c,LH-TL}$ ..... Characteristic Impedance of the LH-TL

v_p ..... Phase Velocity

v_g ..... Group Velocity

$-||$ ..... Anti-Parallel

S ..... Poynting Vector

$\beta_{CRLH-TL}$ ..... Phase Constant of the CRLH-TL

$Z_{c,CRLH-TL}$ ..... Characteristic Impedance of the CRLH-TL

C_c ..... Coupling Capacitance of the CSSR-TL

f_c ..... Cut-off Frequency of the CSRR-TL

Z_B ..... Bloch Impedance

$Z_s(j\omega)$, $Z_p(j\omega)$ ..... Series and Shunt Impedances of the CSRR-TL T-Model

ϕ ..... Phase

$f_L = f_{Z,CSRR}$, $f_H = f_{0,CSRR}$ ..... Lower and Upper Cut-off Frequency of the CSRR-TL LH-Band

Δp ..... Length of a Unit Cell

w ..... Width of a Conventional Microstrip Line

s ..... Spacing between the Coupled Lines

a ..... Width of the Microstrip on the CRLH- and CSRR-TL

b ..... Length of the Fingers and Capacitive Gaps on the CRLH- and CSRR-TL, respectively

c ..... Microstrip Width and Rings Separation on the CRLH- and CSRR-TL, respectively

d ..... Width of the Stub Inductor and the Inner Ring on the CRLH- and CSRR-TL, respectively

e ..... Width of the Outer Ring on CSRR-TL

g ..... Gaps between the Fingers and on the Microstrip of the CRLH- and CSRR-TL, respectively

m ..... Length of the Stub Inductor on CRLH-TL

r ..... Radius of the Inner Concentric Ring on CSRR-TL

V_s ..... Source Voltage

R_s ..... Source Resistance

R_L ..... Load Resistance

R_{NE} ..... Near-End Resistance

R_{FE} ..... Far-End Resistance

I_G ..... Generator Current

I_R ..... Receptor Current

L_G ..... Generator Inductance

C_G ..... Generator Capacitance

L_{GR} ..... Inductance between the Generator and the Receptor

C_{GR} ..... Capacitance between the Generator and the Receptor

V_c ..... Coupled Voltage on the Receptor

V_{in} ..... Input Voltage across the Load

Z_{eq} ..... Equivalent Impedance of the Receptor for the Capacitively Coupled Lines

Z_{CGR} ..... Impedance due to Generator Receptor Capacitive Coupling

Z_{NE} ..... Near-End Impedance

Z_{FE} ..... Far-End Impedance

Z_p ..... Net Impedance of the Receptor's Second Branch for the Capacitively Coupled Lines

V_{NE}^{CAP} ..... Capacitive Near-End Voltage

V_{FE}^{CAP} ..... Capacitive Far-End Voltage

I_1, I_2 ..... Loop Currents in Inductively Coupled Lines

Z_{CL}, Z_{LR} ..... Impedances due to Left and Right Handed Components

Z_{LGR} ..... Impedance due to Generator Receptor Inductive Coupling

Z_{DNE}, Z_{DFE} ..... Near-End and Far-End Impedance Notations used to Simplify Expressions

V_{NE}^{IND} ..... Inductive Near-End Voltage

V_{FE}^{IND} ..... Inductive Far-End Voltage

V_{NE}^{TOT} ..... Near-End Total Voltage

V_{FE}^{TOT} ..... Far-End Total Voltage

$||$ ..... Modulus Operator

$\approx$ ..... Approximate Notation

$RH-/CRLH-TL$ ..... Coupled RH- and CRLH-TLs

$RH-/CSRR-TL$ ..... Coupled RH- and CSRR-TLs

ADS ..... Advanced Design System

$tan\delta$ ..... Loss Tangent

f_{CL} ..... Lower Left-Handed Cut-off Frequency for the CRLH-TLs

f_0, $f_{0,CRLH}$ ..... Transition Frequency from LH-Band to RH-Band of the CRLH-TLs

CHAPTER 1. INTRODUCTION

1.1. Background

Electromagnetic Metamaterials, or commonly known as Metamaterials, are substances which do not exist in nature and are artificially man-made. To be more precise they are artificial effectively homogeneous electromagnetic structures that exhibit some unusual properties that are not easily found in nature. As per the definition, by "effectively homogeneous structures" we mean structures whose overall dimension or size of a single unit cell is much smaller than the guided wavelength λ_g. The overall size should be at least a quarter wavelength smaller that would define the effective-homogeneity condition. If the effective-homogeneity condition is satisfied then the wave propagating inside the metamaterial (MTM) medium will have a refractive phenomenon prevailing over the scattering/diffraction phenomenon. Apart from this the other very important property of metamaterials is determined in terms of the refractive index n given by

$$n = \pm\sqrt{\epsilon_r \mu_r} \tag{1.1}$$

which classifies them into separate categories depending upon the permittivity (ϵ) and permeability (μ) of that medium. One such category of metamaterials that satisfies the aforementioned conditions and requirements are the Left-Handed Metamaterials. The very well-known Left-Handed (LH) structures that we will be going over in this thesis are Composite Right/Left-Handed (CRLH) transmission lines and Complementary Split Ring Resonators (CSRR) [7].

1.2. Motivation for Work

Over the ages as we have been observing the tremendous growth and advancement in technology. Accordingly the need to fulfill those demands is also changing drastically. A very common example that can be looked upon is the area of wireless communications. Today almost every electronic item involves wireless systems to serve our needs better and make life easier in terms of communicating and transmitting information over long and short distances. A rapid increase in use of wireless systems require more RF electronic circuitry to be placed in a manner that occupies less space and at the same time also serve the need of providing better performance and functionality. In order to achieve this, metamaterials due to their unusual behavior have found abundant applications in the fabrication of RF/Microwave devices such as bandpass filters, resonating antennas and directional couplers [2]. A metamaterial that has played a crucial role in

implementing theaforementioned applications are the Left-Handed (LH) structures (i.e. CRLH and CSRR-TLs) [7]-[16].

Up until now, the research and analysis regarding these Left-Handed structures have not been performed in the light of EMC analysis. In this thesis we have addressed this problem by taking a different path, where we are not interested in the coupling between the two transmission lines (i.e. a conventional Right-Handed (RH) and CRLH and the second case being RH and CSRR) for designing power couplers/combiners but, rather interested in determining the coupled noise voltages induced onto the the CRLH-TLs and CSRR-TLs when it is brought in close proximity of the regular conventional Right-Handed (RH) transmission line.

1.3. Problem Statement

In this thesis we will investigate the coupling problem from an EMC analysis point of view and not from intentional coupling which was meant to be in earlier cases (for example when designing a Phase coupling (PC) edge-coupled directional coupler [7]). As it has been mentioned earlier that today many wireless systems involve RF circuitry placed into small areas of the RF boards and if there are some transmission lines running that are quite close to each other then the unintentional coupling would disrupt the overall performance of the system. In order to understand the coupling effects we have first studied the various transmission lines structures, such as CRLH and CSRR-TLs, and then implemented them in real world applications by determining what would be the coupled noise voltages induced onto these lines when they are close to the conventional microstrip line. Furthermore, the parameters that could possibly reduce those noise voltages were determined. Initially, the information on Left-Handed Metamaterials (i.e. CRLH and CSRR) in terms of geometry and the equivalent circuits have been presented in Chapter 2. Chapter 3 then presents the RH-/CRLH and RH-/CSRR TLs equivalent circuits models for a single unit cell and the derived analytical expressions for computing the near-end and far-end coupling voltages. Chapter 4 is the validation of the equivalent circuit models of RH-/CRLH and RH-/CSRR TLs with measurements and simulation results, followed by the design guidelines and tradeoffs in Chapter 5. Finally the conclusion is presented in Chapter 6.

CHAPTER 2. LEFT-HANDED METAMATERIALS: GEOMETRY AND EQUIVALENT CIRCUIT MODELS

2.1. Introduction

This chapter presents two very popular Left-Handed Structures, Composite Right/Left Handed (CRLH) Transmission Lines and a microstrip line based on Complementary Split Ring Resonators (CSRRs). Initially, we will analyze the equivalent circuit models of individual Right and Left-Handed transmission lines that are required building blocks of the aforementioned Left-Handed geometries. Then later in Chapter 3 look into the real problem of coupling by analyzing the equivalent circuit models when each of these Left-Handed structures are coupled to conventional Right-Handed (RH) Transmission Lines.

2.2. Right-Handed and Left-Handed Transmission Lines: Equivalent Circuits and Properties

2.2.1. Right-Handed Transmission Line (RH-TL)

RH-TLs are most commonly used in practice in the form of microstrip and CPW (Coplanar Waveguide). These TLs can be modeled with cascaded distributed L C parameters. Each cell represents a series inductance and a shunt capacitance. The equivalent circuit model of a RH-TL unit cell is shown in Figure 1. In the circuit, L_R and C_R represent the distributed inductive and capacitive parameters of the line, respectively. For this equivalent circuit the propagation constant and the characteristic impedance can be determined using the following equations [2]:

$$\gamma = \sqrt{Z(\omega)Y(\omega)} = \alpha + j\beta \tag{2.1}$$

and

$$Z_c = \sqrt{Z(\omega)/Y(\omega)} \tag{2.2}$$

where $Z(\omega)$ and $Y(\omega)$ represent the impedance and admittance corresponding to series and parallel branch, respectively, and α and β are the attenuation and phase constants, respectively.

If the line is lossless which means the attenuation is zero i.e. ($\alpha = 0$), then the propagation constant is purely an imaginary value, whereas the characteristic impedance is purely real. For the lossless RH-TL

$$Z(\omega) = j\omega L_R \tag{2.3}$$

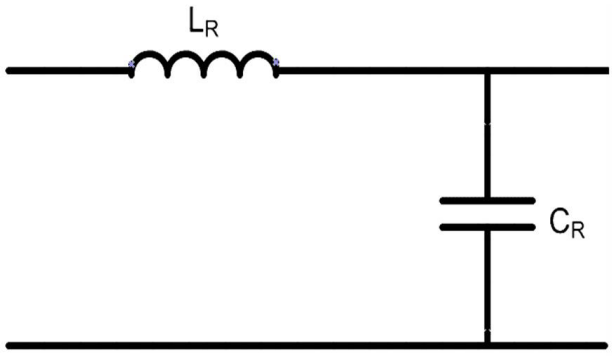

Figure 1. Equivalent Circuit of a Right-Handed Transmission Line Unit Cell.

and

$$Y(\omega) = j\omega C_R. \tag{2.4}$$

By substituting first (2.3) and (2.4) in (2.1) and then in (2.2) we obtain:

$$\beta_{RH-TL} = \omega\sqrt{L_R C_R} > 0 \tag{2.5}$$

and

$$Z_{c,RH-TL} = \sqrt{L_R/C_R}. \tag{2.6}$$

2.2.2. Left-Handed Transmission Line (LH-TL)

Metamaterials are artificial structures exhibiting some unique characteristics under the condition where the period of these structures are much smaller than the guided wavelength (λ_g). The Uniqueness about the Left-Handed metamaterials is that they simultaneously exhibit negative values of effective permittivity and permeability which leads to the backward propagation of waves inside these mediums and also to a negative value of their refractive index [3]. If the aforementioned characteristics can be established in the frequency range of interest, then a LH medium can be obtained. One such medium is the LH-TL that can be realized with the help of distributed L C parameters cascaded into a large number of cells, where each cell represents a series capacitance and a shunt inductance. The unit cell representation of a LH-TL is shown in Figure 2. In the circuit L_L

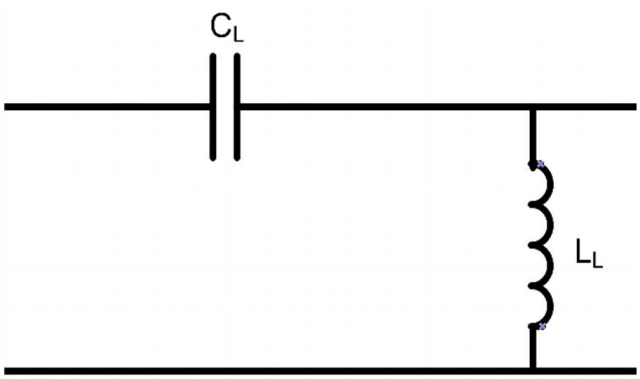

Figure 2. Equivalent Circuit of a Left-Handed Transmission Line Unit Cell.

and C_L represent the distributed inductive and capacitive parameters of the line, respectively. For this equivalent circuit the propagation constant and the characteristic impedance can be determined using the equations (2.1) and (2.2), respectively.

For the LH-TL the series branch impedance and the parallel branch admittance can be written as:

$$Z(\omega) = 1/j\omega C_L \tag{2.7}$$

and

$$Y(\omega) = 1/j\omega L_L. \tag{2.8}$$

By substituting first (2.7) and (2.8) in (2.1) and then in (2.2) we obtain:

$$\beta_{LH-TL} = -1/\omega\sqrt{L_L C_L} < 0 \tag{2.9}$$

and

$$Z_{c,LH-TL} = \sqrt{L_L/C_L}. \tag{2.10}$$

Equations (2.5) and (2.9) represent the dispersion equations for the RH-TL and LH-TL respectively. These equations can be graphically interpreted as shown in Figure 3. If we know the dispersion

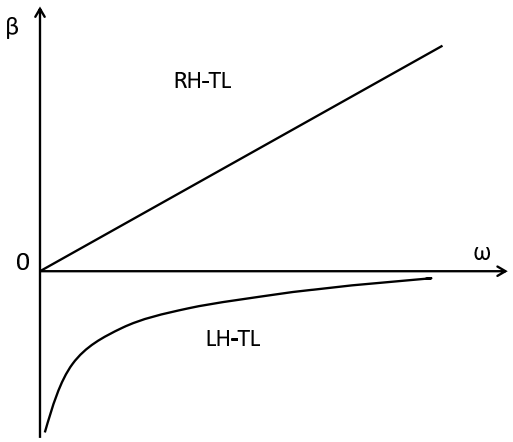

Figure 3. Graphical Interpretation of the Dispersion Equations for RH and LH Lossless Transmission Lines.

equations for the transmission lines we can determine their phase and group velocity accordingly:

$$v_p = \omega/\beta \tag{2.11}$$

and

$$v_g = 1/(d\beta/d\omega) \tag{2.12}$$

where v_p and v_g represent the phase and the group velocity of the line, respectively. From the dispersion equations (2.5) and (2.9) it can be determined that the phase velocity v_p for the RH-TL is positive and negative for the LH-TL, whereas the group velocity v_g is positive for the both RH-TL and the LH-TL. From the above fact it can be concluded that the phase and group velocities for the LH-TL are antiparallel, (i.e. $v_p - || v_g$). The phase velocity v_p tells us about the direction of phase propagation or the wave vector β, whereas the group velocity v_g tells about the direction of power flow or the Poynting vector S as in [7]. Due to the fact that for the LH-TL the phase velocity v_p is negative, the wave propagates in the backward direction in this medium.

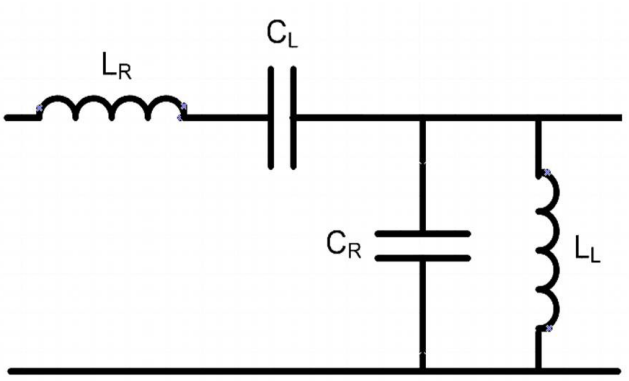

Figure 4. Equivalent Circuit of a Composite Right/Left-Handed Transmission Line Unit Cell.

2.3. Description of the Composite Right/Left-Handed Transmission Line (CRLH-TL)

A Composite Right/Left-Handed Transmission Line is composed of both RH and LH-TLs. Although LH-TLs do not exist in nature, but can be realized practically by loading the conventional microstrip line with the series capacitance and shunt inductance. In order to implement this the equivalent circuit of the conventional microstrip RH-TL is modified in a sense that the series inductance and shunt capacitance are replaced with the series capacitance and a shunt inductance, respectively. A unit cell representation of the CRLH-TL is shown in Figure 4. Here the inductive and capacitive parameters that support the left-handed propagation are represented by L_L and C_L, respectively. The other two parameters L_R and C_R represent the parasitic affects introduced by the conventional microstrip RH-TL. Therefore in order to achieve left-handed propagation on the CRLH-TL, the left-handed parameters (L_L, C_L) should dominate over the right-handed parameters (L_R, C_R).

A CRLH-TL can be implemented by cascading a large number of CRHL-TL cells where the period of these structures is much less then the guided wavelength (λ_g) in the frequency range of interest. For the physical realization of the CRLH-TL, on printed cicuit boards the series capacitance C_L is introduced by interdigitated capacitors and a shunt inductance L_L is introduced by short circuit stubs printed along the length of the transmission line. The layout of a unit cell CRLH-TL is shown in Figure 5.

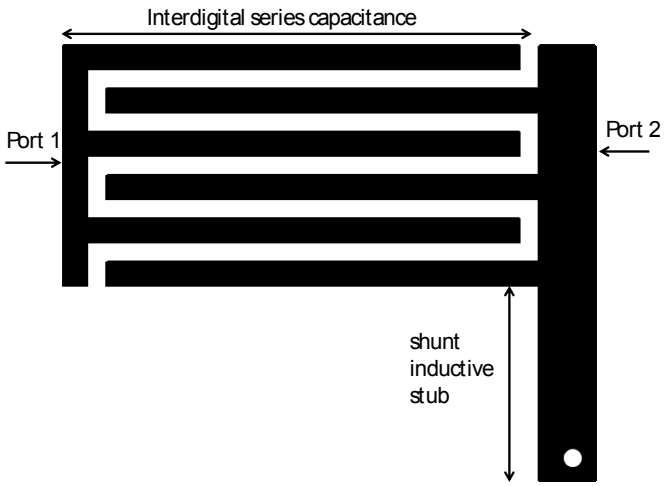

Figure 5. Layout of a CRLH-TL Unit Cell.

Similarly, as for the RH-TL and LH-TL, one can also determine the attenuation constant γ and the characteristic impedance for the CRLH-TL using (2.1) and (2.2) by taking into account the series branch impedance and the parallel branch admittance of the line. The series branch impedance and the parallel branch admittance for the CRLH-TL would be as [2]:

$$Z(\omega) = j(\omega L_R - 1/\omega C_L) \tag{2.13}$$

and

$$Y(\omega) = j(\omega C_R - 1/\omega L_L). \tag{2.14}$$

Next, substituting the above equations (2.13) and (2.14) into (2.1) we get [2]:

$$\beta_{CRLH-TL} = -\sqrt{(\omega L_R - 1/\omega C_L)(\omega C_R - 1/\omega L_L)} < 0 for \omega < \omega_1 \tag{2.15}$$

and

$$\beta_{CRLH-TL} = +\sqrt{(\omega L_R - 1/\omega C_L)(\omega C_R - 1/\omega L_L)} > 0 for \omega > \omega_2 \tag{2.16}$$

where ω_1 and ω_2 represent the minimum and maximum of the series and the parallel resonant circuit in CRLH-TL, respectively, and are given as:

$$\omega_1 = min[1/\sqrt{L_R C_L}; 1/\sqrt{L_L C_R}] \tag{2.17}$$

and

$$\omega_2 = max[1/\sqrt{L_R C_L}; 1/\sqrt{L_L C_R}]. \tag{2.18}$$

If we take a case where $\omega_1 \neq \omega_2$ and $\omega \in (\omega_1, \omega_2)$ then the phase constant β for the CRLH-TL would be an imaginary number, that would result to a real value for the propagation constant. Therefore, this means that the signal propagating on this line would undergo attenuation and thus the circuit will behave as a band pass filter or also called an unbalanced circuit. The other case could be where $\omega_1 = \omega_2$ means there is no stop-band and that would define the balanced circuit. For the balanced case where $\omega_1 = \omega_2$ it is only possible if the following equality is satisfied:

$$L_R C_L = L_L C_R. \tag{2.19}$$

For the balanced case, if we replace ω_1 and ω_2 with ω_0 we get the following expression:

$$\omega_0 = 1/\sqrt{L_R C_L} = 1/\sqrt{L_L C_R} = 1/\sqrt[4]{L_R C_L L_L C_R}. \tag{2.20}$$

Also, for the balanced case from equations (2.15) and (2.16) at ω_0 the phase constant β would be zero.

The overall behavior of the CRLH-TL can be predicted by looking at the above sets of dispersion equations (2.15) and (2.16). Where if $\omega < \omega_1$ (or $\omega < \omega_0$ for the balanced case) then it defines the left-handed propagation region, while if $\omega > \omega_2$ (or $\omega > \omega_0$ for the balanced case) then it defines the right-handed propagation region. The graphical interpretation for these dispersion equations (2.15) and (2.16) can be seen in Figures 6 and 7. The characteristic impedance for the CRLH-TL in an unbalanced circuit can be determined by substituting equations (2.13) and (2.14) in (2.2) which gives:

$$Z_{c,CRLH-TL} = \sqrt{L_L/C_L}.\sqrt{(\omega^2 L_R C_L - 1)/(\omega^2 L_L C_R - 1)} \tag{2.21}$$

and for a balanced circuit by using equation (2.19) in (2.21) we get:

$$Z_{c,CRLH-TL} = \sqrt{L_L/C_L} = \sqrt{L_R/C_R}. \tag{2.22}$$

On comparing equation (2.22) to (2.6), (2.10) we obtain the following relation:

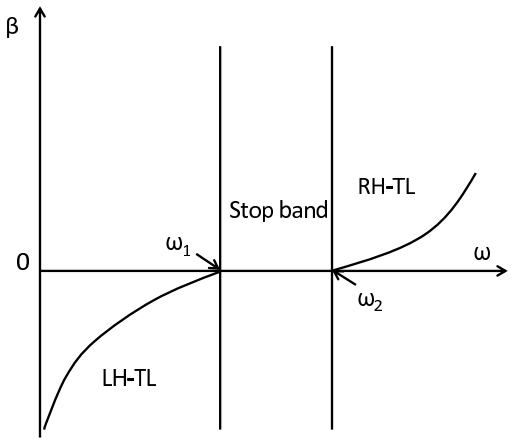

Figure 6. Graphical Interpretation of the Dispersion Equations for Unbalanced CRLH-TL.

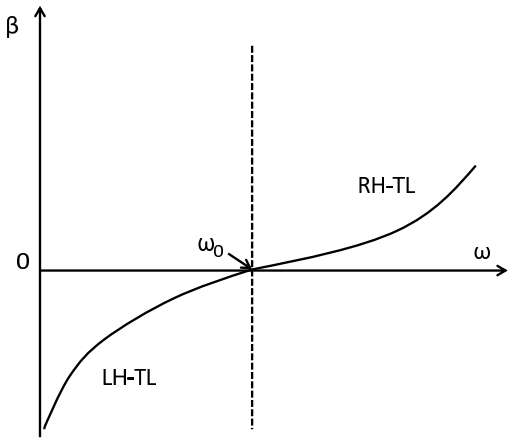

Figure 7. Graphical Interpretation of the Dispersion Equations for Balanced CRLH-TL.

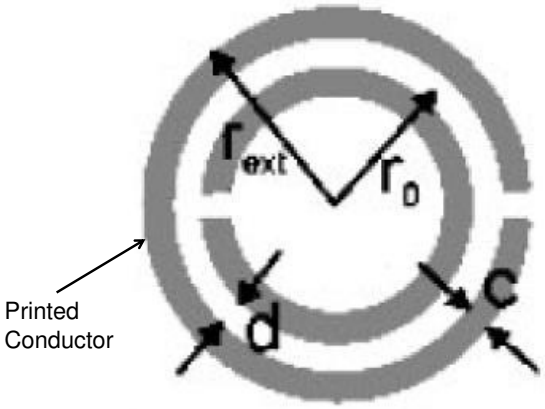

Figure 8. SRR Structural Unit Cell [3].

$$Z_{c,CRLH-TL} = Z_{c,RH-TL} = Z_{c,LH-TL} \tag{2.23}$$

which means that for a balanced CRLH-TL its characteristic impedance is equivalent to that of the RH and LH-TL.

2.4. Description of the Complementary Split Ring Resonators (CSRR's) and Left-Handed Microstrip Lines Based on It.

Before we discuss Complementary Split Ring Resonators (CSRRs), let us first look at Split Ring Resonators (SRRs). SRRs along with a metal thin wire (TWs) were actually the first metamaterial structural units proposed by Pendry at Imperial College, London. Not until 2000 was the first Left-Handed material synthesized by Smith et al. It was designed out of SSRs and TWs as a composite structure into an array which exhibited negative permeability and permittivity values in the desired overlapping frequency ranges. Here SSRs accounted for the negative permeability and the TWs for the negative permittivity of these Left-Handed structures [7].

SSRs are the resonant particles that are used for designing Left-Handed structures with the negative permeability value in the vicinity of the their resonant frequency [3]. The geometry of a SRR unit can be seen in Figure 8. An alternative to these structures are the Complementary Split Ring Resonators (CSRRs) which are just the opposite image of the SRRs and shown in Figure 9. The differing feature about these structures are that they exhibit negative effective permittivity

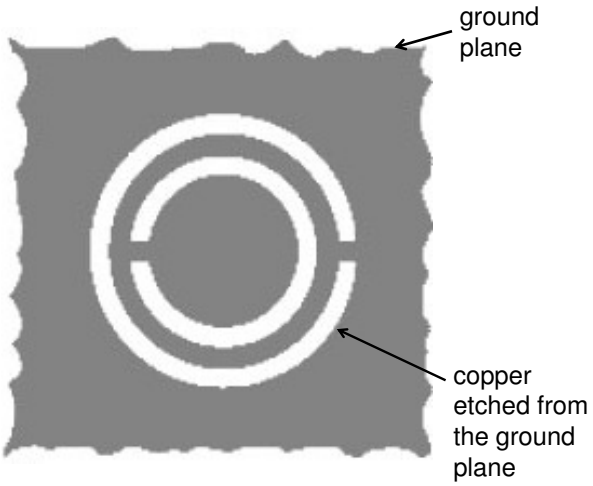

Figure 9. CSRR Structural Unit Cell [3].

instead of permeability (as in the case of SRRs) in the vicinity of their resonant frequency. The other important feature about CSRRs is that they exhibit the same resonant frequency as that of SRRs if the overall dimensions are the same as that of SSRs [3].

Left-Handed metamaterials based on CSRRs are synthesized by first etching CSSRs on the ground plane of a microstrip line, which constitute the bottom layer of the dielectric substrate. By doing so, a negative effective permittivity medium in a narrow band is obtained. In order to achieve left-handedness in the medium, an additional element is required to provide the negative permeability, which can be attained by introducing capacitive gaps in the top conducting layer of the dielectric substrate at periodic intervals. The geometry of a unit cell Left-Handed microstrip line is depicted in Figure 10 with its distributed equivalent circuit (T-model) shown in Figure 11. The first Left-Handed metamaterial based on CSRRs was designed in [4]. The frequency response of the Left-Handed metamaterial provided a narrow band with a sharp cut-off point in the lower end and a smooth transition at the upper end.

The T-model shown in Figure 11 exists only under the condition when the dimension and the spacing between the two adjacent CSSRs are both electrically small. This condition holds true only in the backward propagation region. In order to practically implement a Left-Handed microstrip lines based on CSSRs a large number of unit cells comprising of a microstrip line loaded with CSRRs and

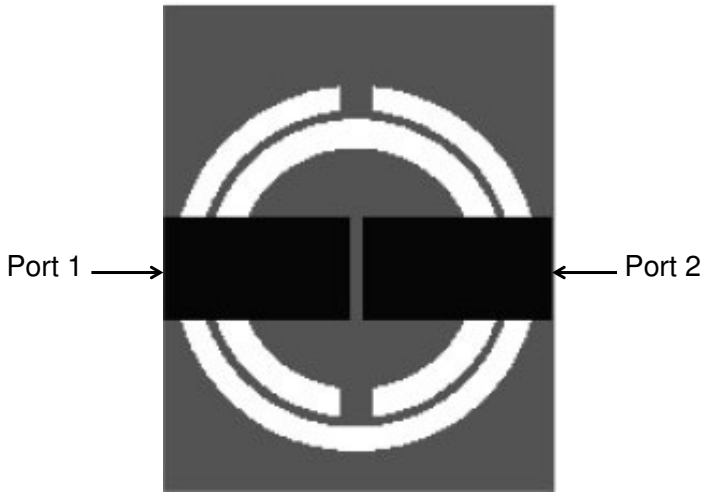

Figure 10. Structural Unit Cell of a Microstrip Transmission Line Loaded with CSRR and a Capacitive Gap [3].

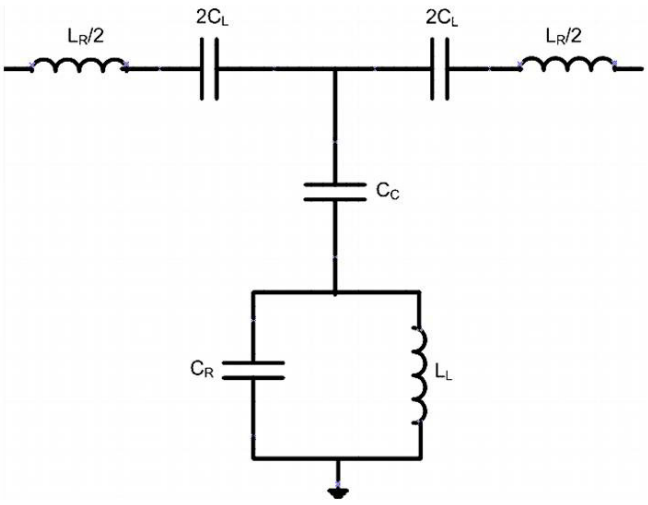

Figure 11. Unit Cell Equivalent Circuit Model of a Microstrip Line Loaded with CSRR and a Capacitive Gap [3].

the capacitive gaps are cascaded. The top conducting layer comprising of series gaps can be modeled as a series equivalent circuit with inductance L_R and gap capacitance C_L, while the CSSRs etched in the bottom (ground) layer can be modeled as a parallel resonant tank circuit with inductance and capacitance denoted as L_L and C_R. These CSSRs units in the bottom layer are coupled to the microstrip host line through capacitance C_c. For this high-pass structure the cut-off frequency (also called the gap-related frequency) f_c should be greater than the intrinsic resonant frequency f_0 of CSRRs. This cut-off frequency is given as [3]:

$$f_c = \frac{1}{2\pi\sqrt{L_R C_L}}. \tag{2.24}$$

This Left-Handed medium that is obtained by cascading a large number of cells is highly dispersive. The Bloch impedance can be written as [3]:

$$Z_B = \sqrt{Z_s(j\omega)[Z_s(j\omega) + 2Z_p(j\omega)]} \tag{2.25}$$

and the phase shift can be written as:

$$cos\phi = 1 + \frac{Z_s(j\omega)}{Z_p(j\omega)} \tag{2.26}$$

where $Z_s(j\omega)$ and $Z_p(j\omega)$ represent the series and the shunt impedances of the T-model, respectively. On substituting the series and the shunt impedances in the above equations (2.25) and (2.26) we get:

$$Z_B = \sqrt{\frac{L_L/C_R}{\frac{1}{C_R\omega} - L_L\omega}\frac{1}{C_L\omega} - \frac{1}{4C_L^2\omega^2} - \frac{1}{C_c C_L \omega^2}} \tag{2.27}$$

and

$$cos\phi = 1 + \frac{1/2C_L\omega}{\frac{1}{C_c\omega} + \frac{L_L/C_R}{L_L\omega - \frac{1}{C_R\omega}}}. \tag{2.28}$$

According to equation (2.28) this medium supports left-handed propagation in that region or over that frequency band where phase, ϕ value comes out to be a real number. With further analysis of the above equation (2.28) the lower and higher end of the band is determined to be [3]:

$$f_L = \frac{1}{2\pi}\frac{1}{\sqrt{L_L(C_R + \frac{4}{\frac{1}{C_L} + \frac{4}{C_c}})}} \tag{2.29}$$

and

$$f_H = \frac{1}{2\pi\sqrt{L_L C_R}}. \tag{2.30}$$

Equations (2.29) and (2.30) defines the lower and higher frequency points where the left-handed propagation exist inside the medium.

CHAPTER 3. NOISE VOLTAGE COUPLING BETWEEN CONVENTIONAL RIGHT-HANDED AND LEFT-HANDED STRUCTURES

3.1. Introduction

In this chapter we will be investigating the desired problem of coupling (i.e. noise voltage coupling) that might occur between two transmission lines printed on a circuit board. Initially, we will analyze this problem by deriving the near- and far-end voltage expressions on the equivalent circuit of the coupled RH- and CRLH-TLs. Later, following the same procedure, the near- and far-end voltages coupled to the CSSR loaded Left-Handed microstrip line will be computed.

3.2. Noise Voltage Coupling between RH-and CRLH-TLs

3.2.1. Layout and the Equivalent Circuit Model for the Coupled RH- and CRLH-TL Unit Cell

The layout of the coupled RH- and CRLH-TL unit cell is shown in Figure 12. The figure defines the problem where a RH-TL of length Δp and width w is coupled to the CLRH-TL separated by a distance s. For simplicity, a symmetrical CRLH-TL is assumed. In this problem the RH-TL is referred as a generator conductor, connected to a source voltage V_s and terminated with a load resistance R_L. The CRLH-TL is referred as a receptor conductor loaded with near-end and far-end resistance R_{NE} and R_{FE}, respectively. The equivalent circuit model is shown in Figure 13 [5] for the layout of the RH- and CRLH-TL in Figure 12. L_G and C_G represents the distributed inductive and capacitive parameters of the RH-TL (generator conductor), respectively. The mutual inductive and capacitive parameters between the RH-TL (generator conductor) and the CRLH-TL (receptor conductor) are denoted as L_{GR} and C_{GR}, respectively.

3.2.2. Analytical Derivations of the Near-End and Far-End Voltages for Capacitively Coupled RH- and CRLH-TLs

The following derivations on near-end and far-end noise voltages that are induced onto the CRLH-TL from the RH-TL will be derived on the basis of two different coupling phenomenon known as capacitive and inductive coupling or weak-coupling. The total coupling will then be determined by summing the effects due to both capacitive and inductive coupling as in [17].

The case of capacitively coupled transmission lines arises when we take into consideration large values of R_L, R_{NE} and R_{FE} resistances that are present in the circuitry. This then results in capacitively coupled RH- and CRLH-TL unit cells. Then, under this condition the general circuit in

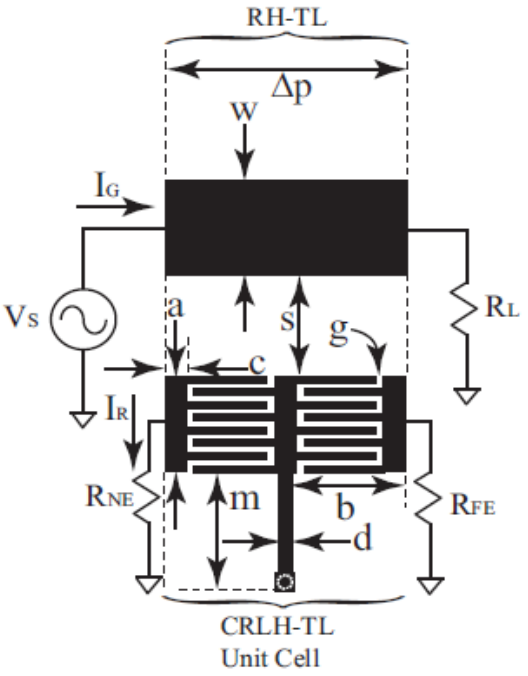

Figure 12. Coupled RH- and CRLH-TLs Unit Cell.

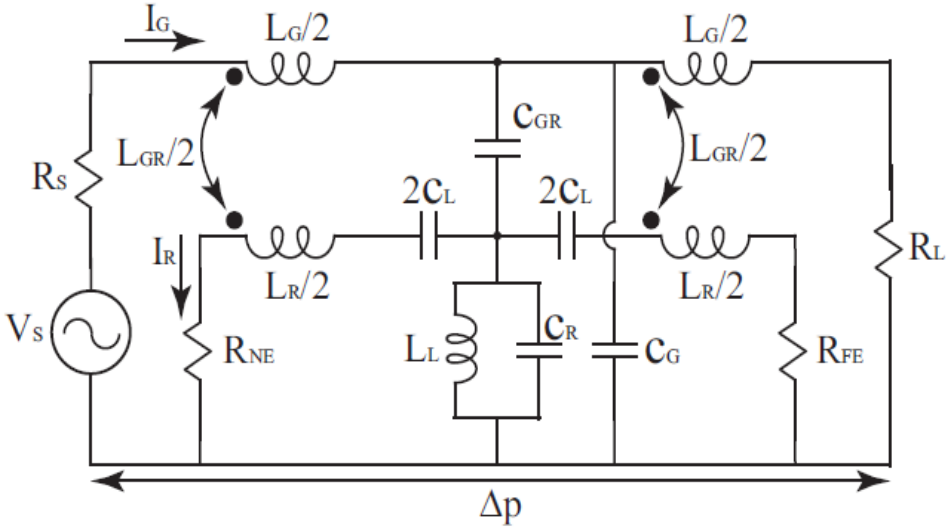

Figure 13. Equivalent Circuit of the Coupled RH- and CRLH-TLs Unit Cell.

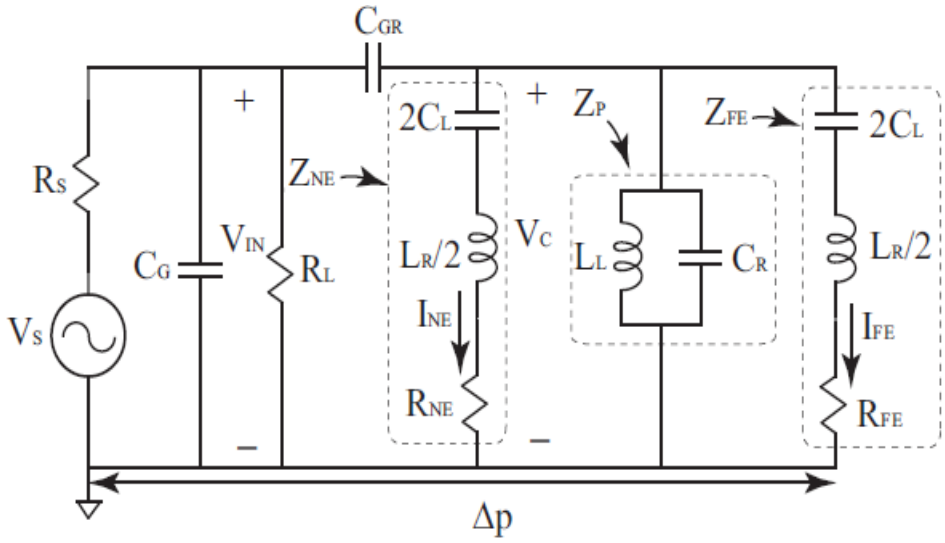

Figure 14. Equivalent Circuit of the Capacitively Coupled RH- and CRLH-TLs Unit Cell.

Figure 13 representing the coupled RH- and CRLH-TL unit cell is reduced to the circuit in Figure 14, which depicts that the coupling between the two unit cells is purely capacitive and represented by C_{GR}. To determine V_C in Figure 14 we can apply voltage division, which gives:

$$V_c = V_{in} \frac{Z_{eq}}{Z_{eq} + Z_{CGR}} \tag{3.1}$$

where Z_{eq} represents the parallel equivalent impedance of the three branches comprising of the right and left-handed components of the CRLH-TL. The first branch includes left-handed capacitance C_L, right-handed inductance L_R and the near-end resistance R_{NE} connected in series. The second branch consists of the left-handed inductance L_L and the right-handed capacitance C_R connected in parallel and the third branch replicates the first due to symmetry except instead of having the near-end resistance it has the far-end resistance R_{FE} . Thus we can express Z_{eq} as:

$$Z_{eq} = \frac{Z_{NE} Z_{FE} Z_P}{Z_{FE} Z_P + Z_{NE} Z_P + Z_{NE} Z_{FE}} \tag{3.2}$$

where Z_{NE}, Z_P and Z_{FE} represents the series near-end, parallel (tank circuit) and the series far-end impedances corresponding to the parallel first, second and the third branch, respectively. The following can be determined by taking the series and parallel impedances of their respective branch comprising of near-end, far-end resistances and the right-/left handed components. These are:

$$Z_{NE} = R_{NE} + \frac{1}{2j\omega C_L} + \frac{j\omega L_R}{2}, \tag{3.3}$$

$$Z_{FE} = R_{FE} + \frac{1}{2j\omega C_L} + \frac{j\omega L_R}{2}, \tag{3.4}$$

and

$$Z_P = \frac{\frac{1}{j\omega C_R} j\omega L_L}{\frac{1}{j\omega C_R} + j\omega L_L}. \tag{3.5}$$

The second term in the denominator of the equation (3.1) represents the impedance due to capacitive coupling between the generator and the receptor conductor which is:

$$Z_{CGR} = \frac{1}{j\omega C_{GR}} \tag{3.6}$$

where C_{GR} is the coupling capacitance between the two lines and the other term V_{in} in (3.1) represents the voltage across the load resistance R_L which can be approximated in terms of source voltage using voltage division as:

$$V_{in} \approx V_s \frac{R_L}{R_L + R_s} \tag{3.7}$$

where V_s and R_s represents the source voltage and source resistance, respectively. Thereafter, the near-end voltage due to capacitive coupling can now be expressed as:

$$V_{NE}^{CAP} = R_{NE} \frac{V_c}{Z_{NE}} \tag{3.8}$$

where R_{NE} is the near-end resistance. Similarly, the far-end voltage can be expressed as:

$$V_{FE}^{CAP} = R_{FE} \frac{V_c}{Z_{FE}} \tag{3.9}$$

where R_{FE} is the far-end resistance.

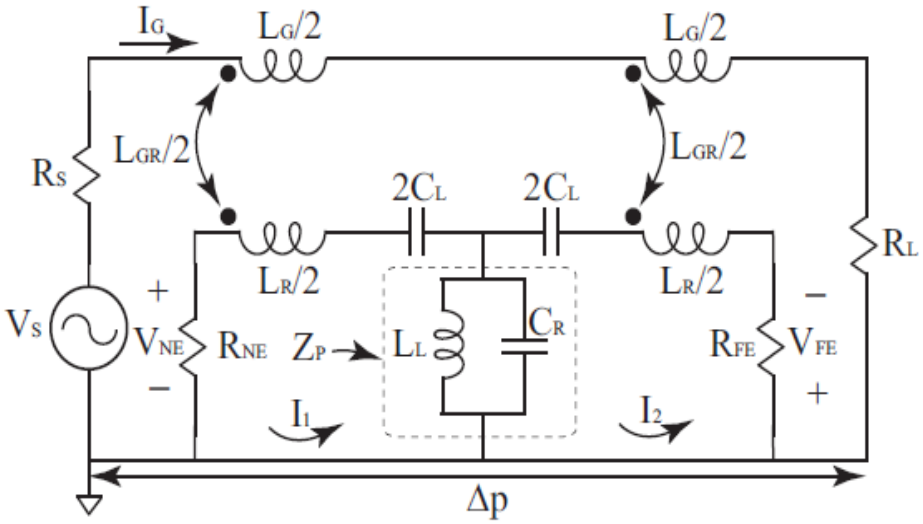

Figure 15. Equivalent Circuit of the Inductively Coupled RH- and CRLH-TLs Unit Cell.

If there exists a condition where $R_{NE} = R_{FE}$ then the near-end voltage due to capacitive coupling is the same as the far-end voltage (i.e. $V_{NE}^{CAP} = V_{FE}^{CAP}$). Under close examination of equations (3.8) and (3.9) it can be determined that the near- and far-end voltages can be reduced by increasing the near-end and far-end impedances Z_{NE} and Z_{FE}, respectively. This can be attained by decreasing the left-handed capacitance C_L or in other words, increasing the spacing between the interdigitated capacitors in the geometry of the CRLH-TL.

3.2.3. Analytical Derivations of the Near-End and Far-End Voltages for Inductively Coupled RH- and CRLH-TLs

In this section we will now analyze the problem of inductive coupling between the RH- and CRLH-TLs. For the investigation of inductively coupled lines, it is assumed that R_L, R_{NE}, and R_{FE} resistance values are small to increase the current on the conductors. This consideration then transforms the general coupling problem circuit between the RH- and CRLH-TL unit cell into the circuit in Figure 15, which depicts that the coupling between the two unit cells is purely inductive and represented by L_{GR}. Throughout the derivation of near- and far-end noise voltages, the following

assumption has been made in the circuit shown in Figure 15:

$$I_G \approx \frac{V_s}{R_s + R_L}. \tag{3.10}$$

Next, we divide the entire circuit into two parts for applying KCL. We denote the left and the right loop as loop 1 and loop 2, respectively, corresponding to current I_1 and I_2, respectively in the circuit. First on applying KCL around loop 1 (left loop) in the circuit we get:

$$Z_{CL}I_1 + Z_{LR}I_1 - I_G\frac{j\omega L_{GR}}{2} + I_1R_{NE} + Z_P(I_1 - I_2) = 0. \tag{3.11}$$

Then, rearranging we get:

$$I_1(R_{NE} + Z_{CL} + Z_{LR} + Z_P) - I_2Z_P - I_G\frac{j\omega L_{GR}}{2} = 0 \tag{3.12}$$

which then eventually leads to the expression:

$$I_1 = \frac{I_2Z_P + I_G\frac{j\omega L_{GR}}{2}}{R_{NE} + Z_{CL} + Z_{LR} + Z_P}. \tag{3.13}$$

Next, if we look at the expression for I_1 in equation (3.13) it can be observed that the second term in the numerator with a factor of I_G, generator current, represents the reactance due to inductive coupling and is denoted as:

$$Z_{LGR} = \frac{j\omega L_{GR}}{2}. \tag{3.14}$$

Thus, equation (3.13) can be rewritten as:

$$I_1 = \frac{I_2Z_P + I_GZ_{LGR}}{Z_{NE} + Z_P} \tag{3.15}$$

where Z_{NE} and Z_P are defined in (3.3) and (3.5), respectively. This then gives:

$$I_1 = \frac{I_2Z_P + I_GZ_{LGR}}{Z_{DNE}} \tag{3.16}$$

where $Z_{DNE} = Z_{NE} + Z_P$. Similarly, applying KCL around loop 2 (right loop) in the circuit gives:

$$R_{FE}I_2 + Z_{LR}I_2 - I_G\frac{j\omega L_{GR}}{2} + Z_{CL}I_2 + Z_P(I_2 - I_1) = 0. \tag{3.17}$$

Then, rearranging we get:

$$I_2(R_{FE} + Z_{CL} + Z_{LR} + Z_P) - I_1 Z_P - I_G \frac{j\omega L_{GR}}{2} = 0 \tag{3.18}$$

and similarly we obtain the expression:

$$I_2 = \frac{I_1 Z_P + I_G \frac{j\omega L_{GR}}{2}}{R_{FE} + Z_{CL} + Z_{LR} + Z_P} \tag{3.19}$$

where the second term in the numerator with a factor of I_G is the inductive coupling reactance Z_{LGR} as in (3.14) and the first three terms of the denominator represents (3.4) of the capacitive coupling. Thus equation (3.19) can be rewritten as :

$$I_2 = \frac{I_1 Z_P + I_G Z_{LGR}}{Z_{FE} + Z_P} \tag{3.20}$$

which is finally represented as:

$$I_2 = \frac{I_1 Z_P + I_G Z_{LGR}}{Z_{DFE}} \tag{3.21}$$

where $Z_{DFE} = Z_{FE} + Z_P$. Now, from equations (3.16) and (3.21) we can determine the final expressions for the loop currents I_1 and I_2 in the circuit by substituting (3.16) into (3.21) or vice-versa. If we substitute equation (3.16) into (3.21) and solve for I_2 we obtain the following sets of equations:

$$I_2 = \frac{\frac{I_2 Z_P + I_G Z_{LGR}}{Z_{DNE}} Z_P + I_G Z_{LGR}}{Z_{DFE}}, \tag{3.22}$$

$$I_2 Z_{DFE} = \frac{I_2 Z_P + I_G Z_{LGR}}{Z_{DNE}} Z_P + I_G Z_{LGR}, \tag{3.23}$$

$$I_2 Z_{DFE} Z_{DNE} = I_2 Z_P^2 + I_G Z_{LGR} Z_P + I_G Z_{LGR} Z_{DNE} \tag{3.24}$$

and on rearranging equation (3.24) we get:

$$I_2(Z_{DFE} Z_{DNE} - Z_P^2) = I_G Z_{LGR} Z_P + I_G Z_{LGR} Z_{DNE}. \tag{3.25}$$

Then finally we obtain the expression for I_2 as:

$$I_2 = \frac{I_G Z_{LGR}(Z_P + Z_{DNE})}{Z_{DFE} Z_{DNE} - Z_P^2}. \tag{3.26}$$

Similarly, on back substituting equation (3.21) into (3.16) we obtain the expression for I_1 as:

$$I_1 = \frac{I_G Z_{LGR}(Z_P + Z_{DFE})}{Z_{DFE}Z_{DNE} - Z_P^2}. \tag{3.27}$$

Thus, we can now determine the near- and far-end voltages due to inductive coupling as:

$$V_{NE}^{IND} = I_1 R_{NE} \tag{3.28}$$

and

$$V_{FE}^{IND} = I_2 R_{FE}. \tag{3.29}$$

Under special circumstances if $R_{NE} = R_{FE}$, then $V_{NE}^{IND} = V_{FE}^{IND}$.

3.2.4. Total Coupling between the RH- and CRLH-TLs

Finally, the total coupling in terms of noise voltages between the transmission lines can be approximately determined by using the results obtained from the capacitive - inductive model [17]. Therefore, the total near- and far-end coupling noise voltages between the RH- and CRLH-TL can be approximately summed as the near-end and far-end noise voltages due to capacitive and inductive coupling in the following manner [17]:

$$V_{NE}^{TOT} = V_{NE}^{CAP} + V_{NE}^{IND} \tag{3.30}$$

and

$$V_{FE}^{TOT} = V_{FE}^{CAP} + V_{FE}^{IND}. \tag{3.31}$$

Next, in order to get the idea of the amount of noise voltages being coupled to the CRLH-TL from the conventional microstrip RH-TL, the analytical expression in (3.30) for near-end noise voltages was computed in Matlab [19] and verified with the circuit simulation results in Designer for a single unit cell. For this computation the values of different circuit elements and parameters were adopted from the RH-/CRLH-phase coupler in [7]. The values were as follows: $V_s = 1.0\ V$, $R_s = 50\ \Omega$, $C_G = 0.33\ pF$, $C_{GR} = 0.33\ pF$, $L_R = 1.1\ nH$, $C_R = 0.45\ pF$, $L_L = 3.04\ nH$, $C_L = 1.3\ pF$, $L_{GR} = 0.13\ nH$, $L_G = 0.825\ nH$, $R_{NE} = 200\ \Omega$ and $R_{FE} = 200\ \Omega$ which showed a significant amount of noise voltages being coupled to the receptor conductor. This can be seen in Figures 16, 17 and 18 for various combinations of R_L, R_{NE}, R_{FE} where $R_{NE} = R_{FE} = 200\ \Omega$ and $R_L = 20$, 200, $2K\ \Omega$. A combination where R_L has values 20, 200, $2K\ \Omega$ and $R_{NE} = R_{FE} = 20\ \Omega$ describes

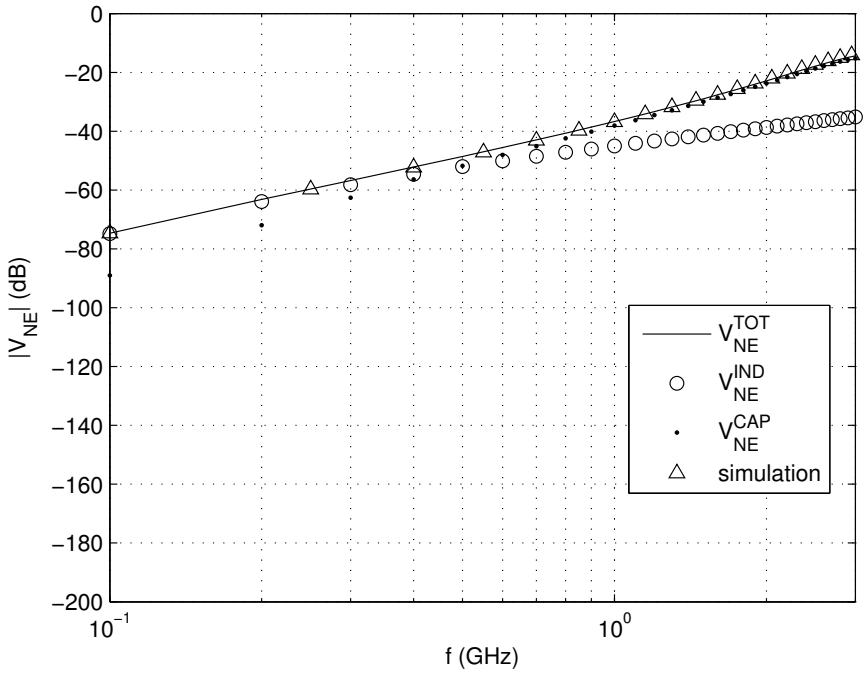

Figure 16. Analytical Computation and Circuit Simulation Results of the General Coupling Circuit for $R_L = 20\ \Omega$.

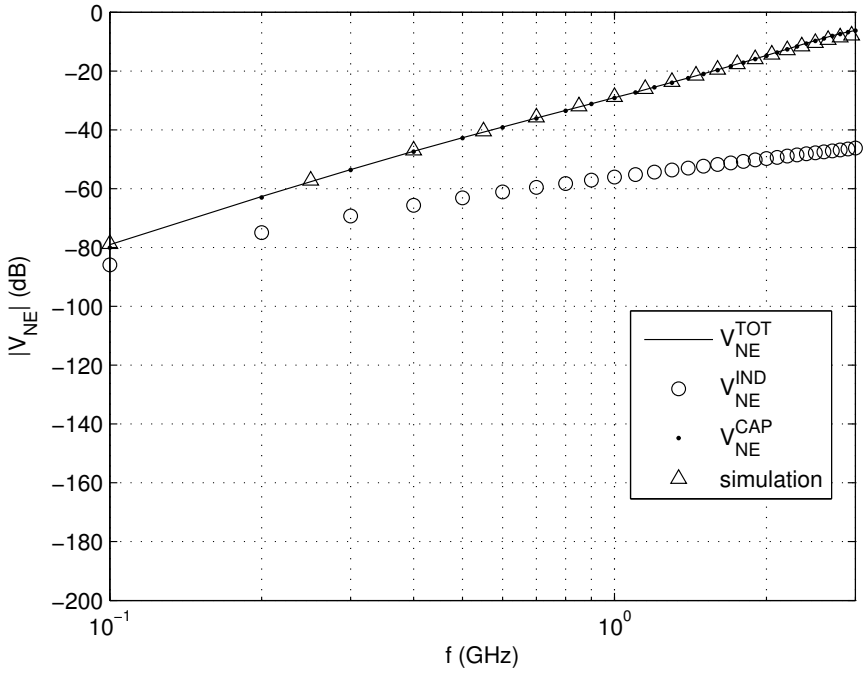

Figure 17. Analytical Computation and Circuit Simulation Results of the General Coupling Circuit for $R_L = 200\ \Omega$.

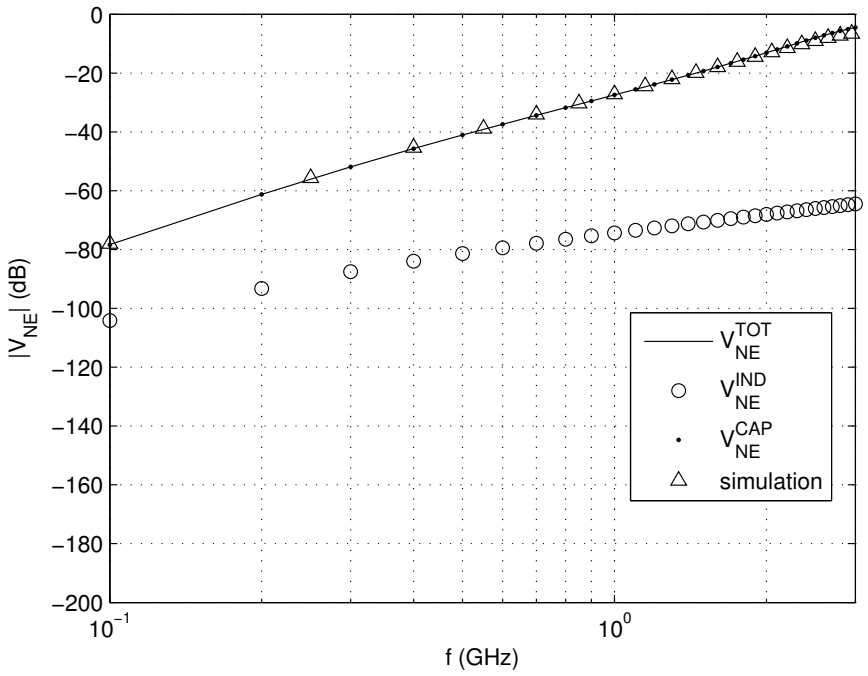

Figure 18. Analytical Computation and Circuit Simulation Results of the General Coupling Circuit for $R_L = 2\ K\Omega$.

a case where the inductive coupling is dominant. The other case being where again R_L = 20, 200, $2K\ \Omega$ and $R_{NE} = R_{FE} = 2K\ \Omega$ describes a case where capacitive coupling is dominant.

3.2.5. Transition Condition from Inductive to Capacitive Coupling

For frequencies below $500MHz$, it is shown in Figure 16 that the inductive coupling is dominant while for frequencies above $500MHz$, the capacitive coupling is dominant. This then, corresponds to equation (3.30) where for frequencies $f < 500MHz$, V_{NE}^{IND} is dominant while for frequencies $f > 500MHz$, V_{NE}^{CAP} is dominant. Thus, in order to determine this transition frequency, it can be obtained by comparing equation (3.8) to (3.28). Before making this comparison we will rearrange the terms in equation (3.8) and make several substitutions. This then results in the following form of (3.8):

$$V_{NE}^{CAP} = \frac{R_{NE}}{Z_{NE}} V_s \frac{R_L}{R_L + R_S} \frac{Z_{eq}}{z_{eq} + Z_{CGR}} \tag{3.32}$$

where the expression in (3.1) for V_c was used. Similarly, in equation (3.28) first we substitute for I_1

using (3.27) and get the following:

$$V_{NE}^{IND} = \frac{I_G Z_{LGR}(Z_P + Z_{DFE})}{Z_{DFE}Z_{DNE} - Z_P^2} R_{NE}. \tag{3.33}$$

Then substituting for I_G using (3.10), $Z_{DFE} = Z_{FE} + Z_P$ and $Z_{DNE} = Z_{NE} + Z_P$ gives:

$$V_{NE}^{IND} = \frac{V_s}{R_s + R_L} \frac{Z_{LGR}(Z_P + Z_{FE} + Z_P)}{(Z_{FE} + Z_P)(Z_{NE} + Z_P) - Z_P^2} R_{NE}. \tag{3.34}$$

Then on further solving and rearranging we get the following:

$$V_{NE}^{IND} = R_{NE} \frac{V_s}{R_s + R_L} \frac{Z_{LGR}(2Z_P + Z_{FE})}{(Z_{NE}Z_P + Z_{FE}Z_P + Z_{NE}Z_{FE})}. \tag{3.35}$$

Next, comparing equation (3.35) to (3.32) and rearranging we get:

$$V_{NE}^{IND} = \frac{R_{NE}}{Z_{NE}} \frac{Z_{NE}}{R_L} R_L \frac{V_s}{R_s + R_L} \frac{Z_{LGR}(2Z_P + Z_{FE})(Z_{NE}Z_{FE}Z_P)}{(Z_{NE}Z_{FE}Z_P)(Z_{NE}Z_P + Z_{FE}Z_P + Z_{NE}Z_{FE})} \tag{3.36}$$

where $\frac{Z_{NE}Z_{FE}Z_P}{Z_{NE}Z_P + Z_{FE}Z_P + Z_{NE}Z_{FE}} = Z_{eq}$ as in equation (3.2). Therefore (3.35) can be rewritten and rearranged as:

$$V_{NE}^{IND} = \frac{R_{NE}}{Z_{NE}} V_s \frac{R_L}{R_L + R_s} \frac{Z_{LGR}}{R_L} \frac{(2Z_P + Z_{FE})Z_{eq}}{Z_{FE}Z_P}. \tag{3.37}$$

Now, comparing equation (3.32) to (3.37) we get:

$$\frac{1}{Z_{eq} + Z_{CGR}} = \frac{Z_{LGR}(2Z_P + Z_{FE})}{R_L Z_{FE} Z_P}. \tag{3.38}$$

By further taking the absolute value on both sides and making an assumption that $Z_{eq} + Z_{CGR} \approx Z_{CGR}$ gives:

$$|\frac{R_L}{Z_{CGR}}| \approx |Z_{LGR}||\frac{2Z_P + Z_{FE}}{Z_{FE}Z_P}|. \tag{3.39}$$

Then rearranging again finally leads to the following expression that defines the condition where the near-end transition frequency occurs:

$$|Z_{LGR}Z_{CGR}| \approx |\frac{R_L Z_{FE} Z_P}{Z_{FE} + 2Z_P}|. \tag{3.40}$$

A closer look at (3.40) reveals that there are a few things that should be taken into account, such as consideration of both inductive- and capacitive-shielding of a CRLH-TL in the case of

unintentional coupling and it shows that the capacitive coupling could be dominant in a certain limited band whereas the inductive coupling would be dominant in the remaining band. It should also be mentioned that the transition frequency strongly depends on the value of load resistance R_L. Finally, similar expressions for the far-end can also be determined.

3.3. Noise Voltage Coupling between RH- and CSRRs Based LH-TLs

3.3.1. Layout and the Equivalent Circuit Model for the Coupled RH- and CSRR-TL Unit Cell

The unit cell layout of the coupled RH- and CSRR-TLs is depicted in Figure 19. Similar, to Figure 12, the following figure now defines the problem where a RH-TL of length Δp and width w is coupled to the microstrip line loaded with CSRR and capacitive gaps, separated by a distance s. The CSRRs are etched onto the bottom ground layer while the capacitive gaps onto the top conducting layer of the dielectric substrate. For simplicity, a symmetrical CSRR-TL is assumed. Likewise, in the previous problem, the RH-TL is referred as a generator conductor, connected to a source voltage V_s and terminated with a load resistance R_L. The CSRR-TL is referred to as a receptor conductor loaded with near-end and far-end resistances R_{NE} and R_{FE}, respectively. The equivalent circuit model is shown in Figure 20 [5] for the layout of the RH- and CSRR-TLs in Figure 19. Where again L_G and C_G represents the distributed inductive and capacitive parameters of the RH-TL (generator conductor), respectively. The mutual inductive and capacitive parameters between the RH-TL (generator conductor) and the CSRR-TL (receptor conductor) are denoted as L_{GR} and C_{GR}, respectively.

3.3.2. Analytical Derivations of the Near-End and Far-End Voltages for Capacitively Coupled RH- and CSRR-TLs

As for the case of coupled RH- and CRLH-TLs a similar kind of approach was followed to determine the near-end and far-end noise voltages that are induced onto the CSRR-TL from the RH-TL due to capacitive and inductive coupling. Then, the total coupling due to both capacitive and inductive coupling will determine the total near- and far-end noise voltages in [17].

Here initially we will investigate the capacitive coupling between the RH- and CSRR-TL unit cell for large values of R_L, R_{NE} and R_{FE}. Thus, for the capacitively coupled transmission lines the general circuit in Figure 20 representing the coupled RH- and CSRR-TL unit cell is reduced into the circuit shown in Figure 21. This depicts that the coupling between the two unit cells is capacitive.

If we were to compare the two capacitively coupled models in Figures 14 and 21 corresponding to the RH-/CRLH-TL, and RH-/CSRR-TL we observe that the later is just the replicate of the

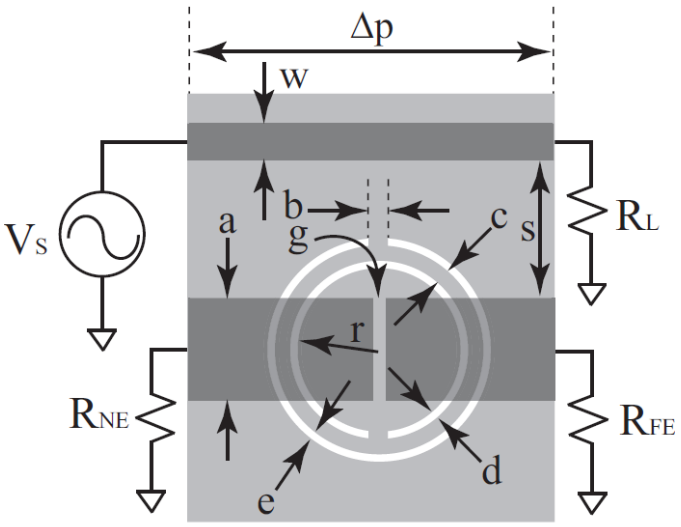

Figure 19. Coupled RH- and CSRR-TLs Unit Cell.

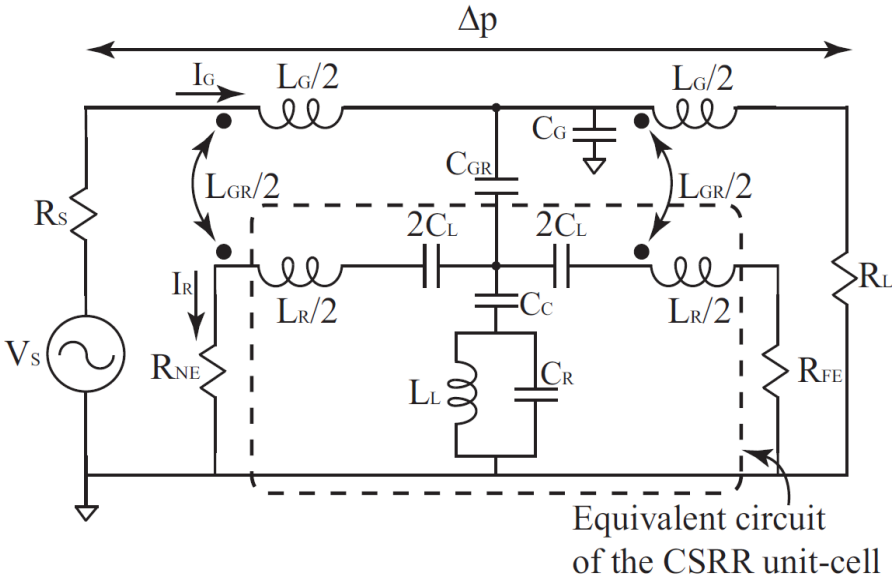

Figure 20. Equivalent Circuit of the Coupled RH- and CRSRR-TLs Unit Cell.

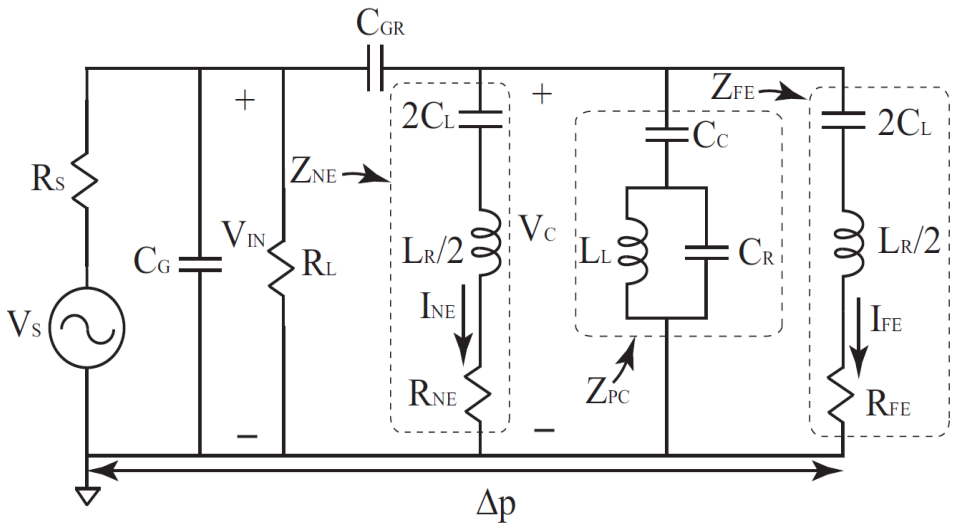

Figure 21. Equivalent Circuit of the Capacitively Coupled RH- and CSRR-TLs Unit Cell.

former, with the only change in the second branch of the parallel equivalent impedance Z_{eq}. Where the second branch net impedance is denoted as Z_p. Therefore, under this observation the equivalent circuit model for RH- and CSRR-TL would also lead to similar expressions for the near- and far-end noise voltages with the only exception of different expression for the impedance parameter Z_p.

Following the similar procedure as outlined for the RH-/CRLH-TL, first, we determine the coupled voltage V_c onto the CSRR-TL using the voltage division that would correspond to equation (3.1). The parallel equivalent impedance Z_{eq} still corresponds to the net impedances of the three branches Z_{NE}, Z_P and Z_{FE} as stated in equation (3.2). The only difference being that the impedance parameter Z_P would now be modified to include the impedance of C_c. C_c is the coupling capacitance between the top conducting layer with capacitive gaps and the bottom ground layer with CSRRs. Thus, the modified Z_P can be expressed as:

$$Z_P = \frac{1}{j\omega C_c} + \frac{\frac{1}{j\omega C_R} j\omega L_L}{\frac{1}{j\omega C_R} + j\omega L_L} \tag{3.41}$$

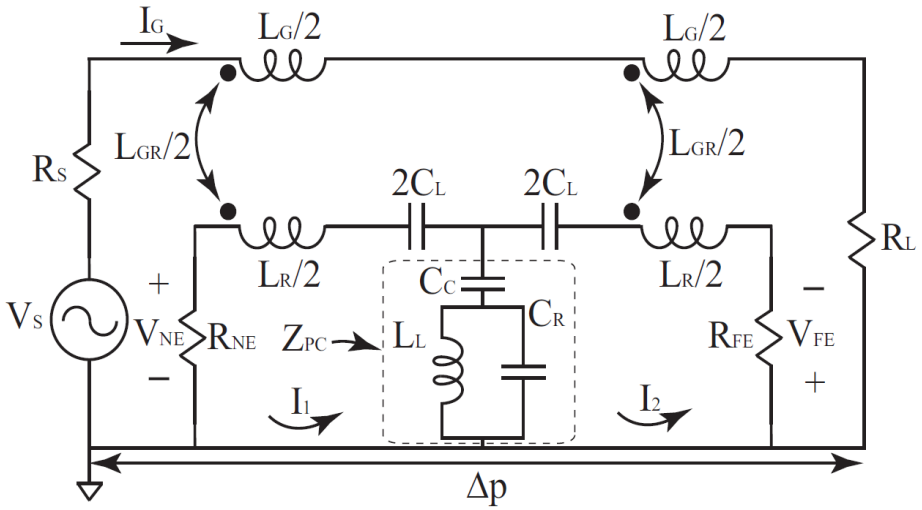

Figure 22. Equivalent Circuit of the Inductively Coupled RH- and CSRR-TLs Unit Cell.

whereas the expression for Z_{NE} and Z_{FE} would not change and still correspond to the equations (3.3) and (3.4), respectively.

Similarly, the term Z_{CGR} of the equation (3.1) for the case of RH-/CSRR-TL would still represent the impedance due to capacitive coupling between the generator and the receptor conductor corresponding to equation (3.6). The only difference being that the receptor would now be a CSRR-TL instead of CRLH-TL. The other term being V_{in}, that defines the voltage across the load resistance R_L would again exactly correspond to equation (3.7). Thus, from all the aforementioned observations and interpretations the near- and far-end noise voltages that are induced onto the CSRRs-TL from the RH-TL would correspond to the expressions similar to RH- and CRLH-TL as defined by equations (3.8) and (3.9), respectively.

3.3.3. Analytical Derivations of the Near-End and Far-End Voltages for Inductively Coupled RH- and CSRR-TLs

In this section we will again analyze the problem of inductive coupling between the RH- and CSRR-TL. As already mentioned earlier, in order to examine the inductively coupled lines R_L, R_{NE}, and R_{FE} resistance values should be small enough to support inductive coupling. This consideration

then transforms the general coupling problem circuit between the RH- and CSRR-TL unit cell into the circuit shown in Figure 22. This depicts that the coupling between the two unit cells is inductive.

If we now compare the two inductively coupled models corresponding to the RH-/CRLH-TL and RH-/CSRR-TL, the entire circuitry remains the same except in the shunt elements where now, an extra capacitive component has been introduced in series with the tank circuit. This capacitive component corresponds to the coupling capacitance C_c between the top conducting layer with capacitive gaps and the bottom ground layer with CSSRs etched onto it. The net impedance of this shunt, denoted as Z_P, corresponds to equation (3.41).

Finally, a similar procedure is followed for the inductively coupled RH- and CSRR-TLs for deriving the near- and far-end noise voltage expressions as outlined in the case of RH- and CRLH-TL. The results are the same expressions as in (3.28) and (3.29) except Z_P is redefined in (3.41).

3.3.4. Total Coupling between the RH- and CSRR-TLs

Finally, the total coupling in terms of noise voltages between the RH- and CSRR-TL can be approximated as the sum of the noise voltages due to capacitive and inductive coupling for the near- and far-end, respectively. This can be shown as in equations (3.30) and (3.31) where again Z_P is redefined in (3.41).

CHAPTER 4. VALIDATION OF THE COUPLED RH- AND CRLH EQUIVALENT CIRCUIT MODELS AND THE RH- AND CSRR EQUIVALENT CIRCUIT MODELS

4.1. Introduction

After deriving the expressions for the induced noise voltages corresponding to the equivalent circuit models of RH-/CRLH-TL and RH-/CSRR-TL unit cells the next step would be to validate these models. This will be shown with the help of simulation and measurements results. In order to validate these models, we will use 7 unit cells of the CRLH- and CSSR-TLs each, coupled to the conventional microstrip RH-TL as shown in Figures 23 and 24. First, 7 unit cells of the RH- and CRLH-TL will be presented, followed by 7 unit cells of the RH- and CSRR-TL.

4.2. 7 Unit Cells of the Coupled RH- and CRLH Transmission Lines

For the validation of the equivalent circuit model of the RH- and CRLH-TL and an accurate modeling of the coupling, three different test cases were simulated, manufactured and tested. Each test case, of different dimensions were chosen in order to investigate the accuracy of the equivalent circuit model.

4.2.1. Layout of Different Cases

The Layout of the three test cases that were chosen correspond to a drawing shown in Figure 23. These cases were selected in a manner such that the different dimensions in each case would corresponds to the left-handed components of the CLRH-TL. Case 1 had a stub inductor length of m = 4.75 mm, and an interdigital capacitors spacing of g = 0.25 mm, whereas case 2 shown had a longer stub inductor of length m = 9.75 mm, while the spacing between the interdigital capacitors was kept to be the same. Case 3 had an inductor stub length of approximately the same length as case 2 of m = 8.85 mm, while the spacing between the interdigital capacitors was increased to g = 0.35 mm. Thus, case 2 was used to validate the accuracy of the equivalent circuit model for different values of shunt inductance L_L and case 3 was used for validating the accuracy of the model for the different values of the series interdigital capacitance C_L.

4.2.2. Simulation and Measurement Results

The single unit cell for the coupled RH- and CRLH-TLs was simulated first for cases 1, 2 and 3 in Momentum [20]. Each case was designed with the specified dimensions corresponding to the notations used in Figure 12. For case 1 the dimensions were: a = 5.25 mm, b = 10.4 mm, c = 0.5 mm, d = 0.5 mm, g = 0.25 mm, m = 4.75 mm, Δp = 21.42 mm, s = 10 mm, w = 4.8 mm. For

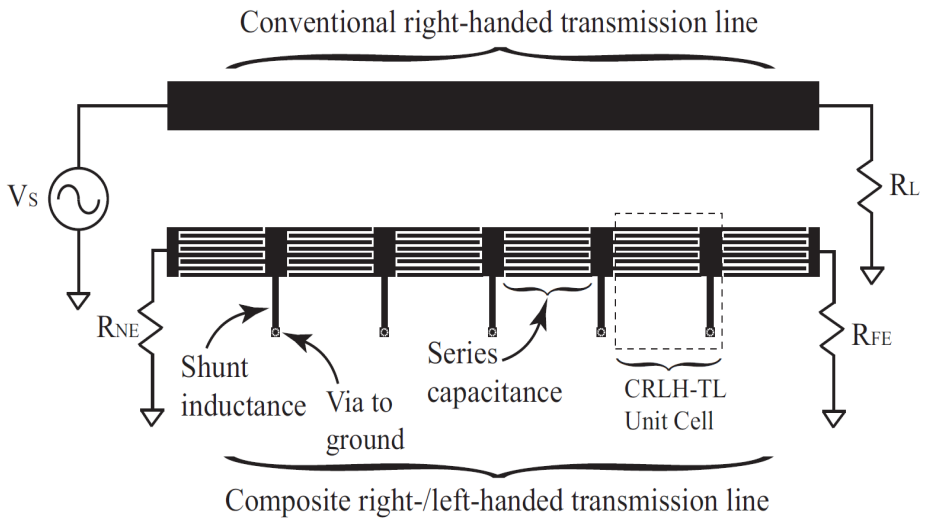

Figure 23. Coupled Conventional Right-Handed and Composite Right-/Left-Handed Transmission Lines.

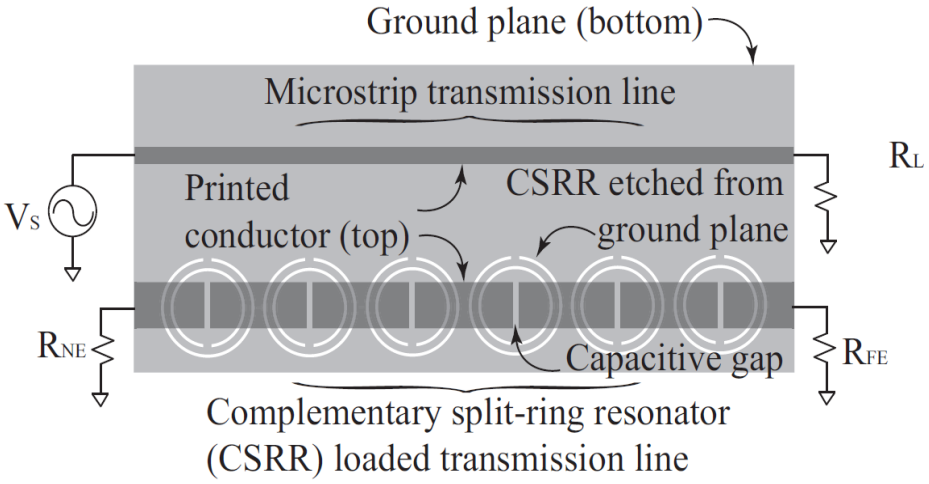

Figure 24. Coupled Conventional Right-Handed and Complementary Split Ring Resonator Transmission Lines.

Table 1. Extracted Equivalent Circuit Values for the Coupled RH- and CRLH-TL Unit Cells.

Value	Case 1	Case 2	Case 3
L_R (nH)	2.22	2.22	2.22
C_L (pF)	1.57	1.57	0.99
L_L (nH)	3.4	6.12	6.12
C_R (pF)	1.65	1.65	1.65
L_G (nH)	2.2	2.2	2.2
C_G (pF)	0.94	0.94	0.99
L_{GR} (nH)	0.059	0.059	0.089
C_{GR} (pF)	0.0274	0.0196	0.0117

Table 2. Optimized Equivalent Circuit Values for the Coupled RH- and CRLH-TL Unit Cells.

Value	Case 1	Case 2	Case 3
L_R (nH)	2.30	2.30	2.30
C_L (pF)	1.49	1.49	1.08
L_L (nH)	3.14	5.50	5.20
C_R (pF)	1.60	1.60	1.60
L_G (nH)	2.4	2.4	2.4
C_G (pF)	0.92	0.92	0.825
L_{GR} (nH)	0.063	0.063	0.089
C_{GR} (pF)	0.0290	0.0184	0.0114

case 2: a = 5.25 mm, b = 10.4 mm, c = 0.5 mm, d = 0.5 mm, g = 0.25 mm, m = 9.75 mm, Δp = 21.42 mm, s = 10 mm, w = 4.8 mm. Finally, for case 3: a = 6.15 mm, b = 10.4 mm, c = 0.5 mm, d = 0.5 mm, g = 0.35 mm, m = 8.85 mm, Δp = 21.42 mm, s = 10 mm, w = 5.7 mm. Δp and s correspond to the length of the RH- and CRLH unit cell and the spacing, respectively, which has been kept constant throughout all the cases.

After, unit cells were simulated in ADS Momentum, the S-parameters were used to extract the equivalent circuit models of each unit cell. This was achieved using the matrix method described in [7]. The extracted circuit values and optimized circuit values for the three case are shown in Tables 1 and 2, respectively. Next, to model the layouts for each case, seven equivalent circuits representing each unit cell in the layout were interconnected. A picture of the equivalent circuit in Designer is shown in Figure 25. The terminations R_L, R_{NE}, and R_{FE}, were defined to be 50 Ω. The Full-wave and equivalent-circuit simulation results are shown in Figures 26, 27 and 28. Finally, these coupled transmission lines were then printed on a 1.575 mm thick Rogers RT/duroid 5880 (ϵ_r = 2.2, tan δ = 0.0009) [21] substrate and are shown in Figures 29, 30 and 31 for cases 1, 2 and 3, respectively. A picture of the device under test can be seen in Figures 32 for near-end coupling using

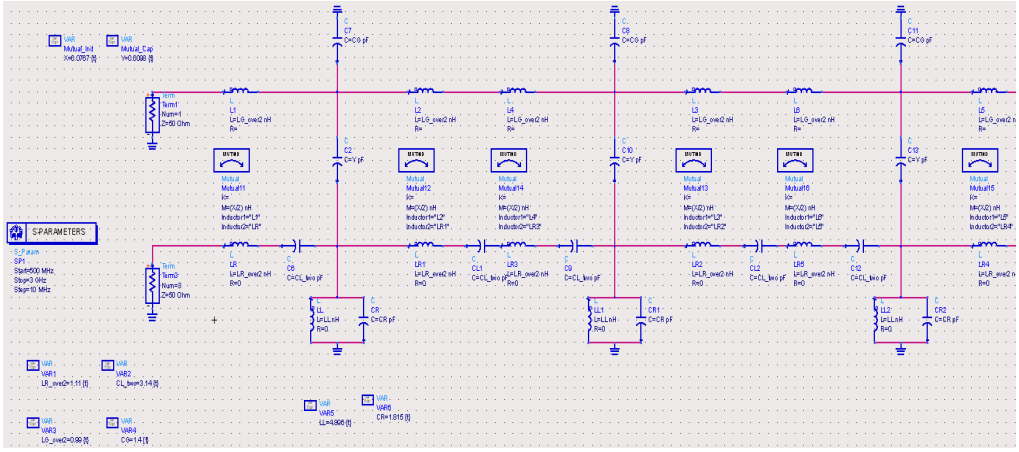

Figure 25. Circuit Equivalent of the Seven Unit Coupled RH- and CRLH-TLs in Designer.

an Agilent ENA series network analyzer. The ports not being used are terminated with 50 Ω load. The measurement results obtained for each case are shown in Figures 26, 27 and 28. The results in Figures 26, 27 and 28 show that the equivalent circuit in Figure 13 can be used to accurately model the coupling between the RH-and CRLH-TL. Since, the analytical expressions obtained in equations (3.30) and (3.31) were derived directly from this circuit, it shows that these expressions can be used to compute the per-unit near- and far-end noise voltages induced onto the CRLH-TL from the conventional microstrip RH-TL. A similar observation in terms of overall agreement was also made for the far-end voltages.

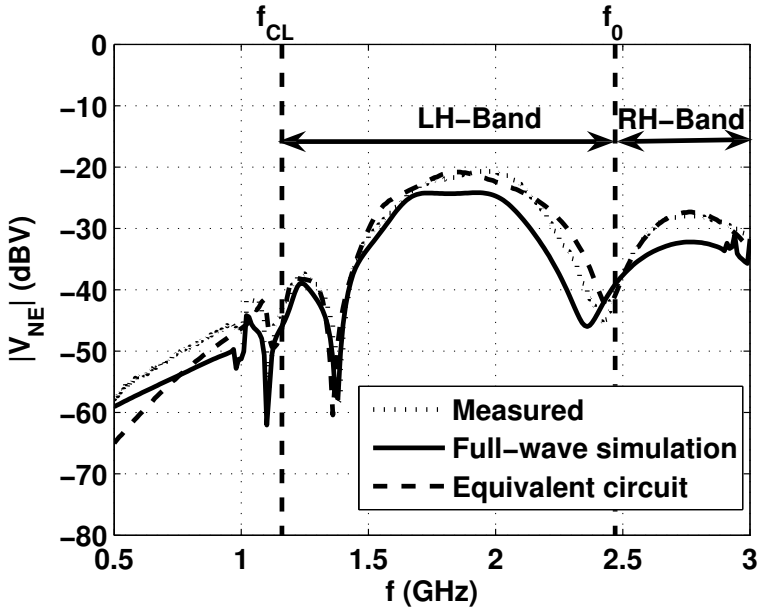

Figure 26. Near-End Voltage Measurement and Simulation Results for Case 1.

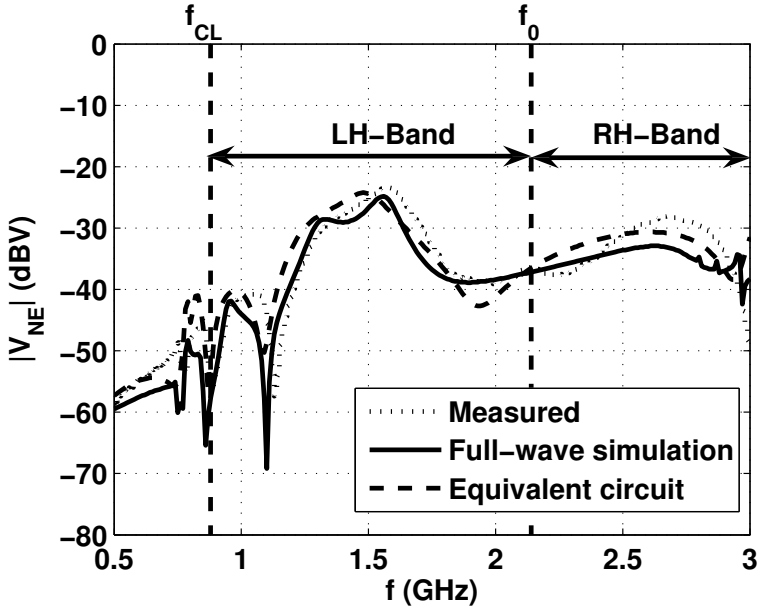

Figure 27. Near-End Voltage Measurement and Simulation Results for Case 2.

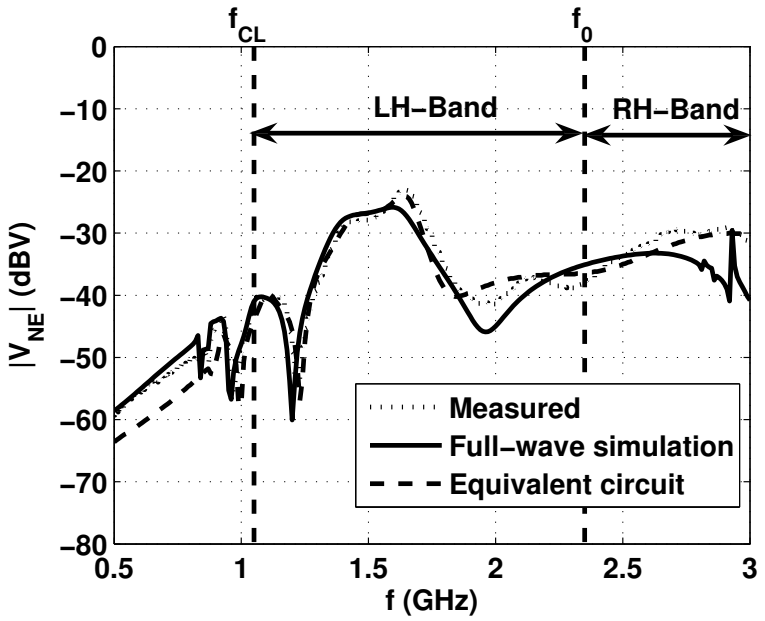

Figure 28. Near-End Voltage Measurement and Simulation Results for Case 3.

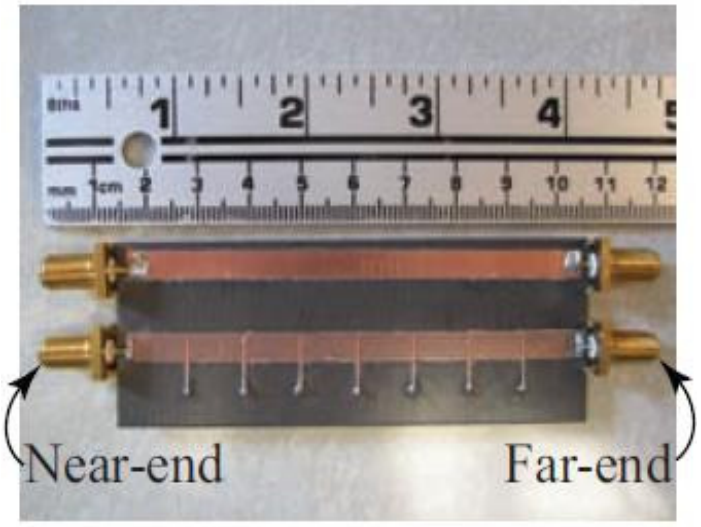

Figure 29. Photograph of the Manufactured Seven Unit Cell RH-/CRLH Coupled Transmission Lines for Case 1.

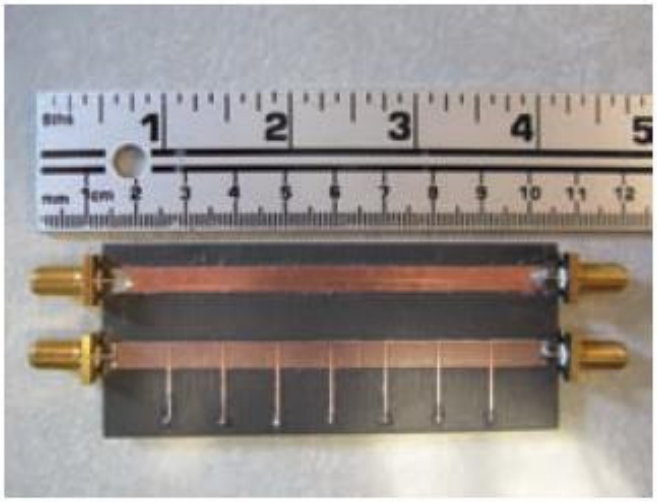

Figure 30. Photograph of the Manufactured Seven Unit Cell RH-/CRLH Coupled Transmission Lines for Case 2.

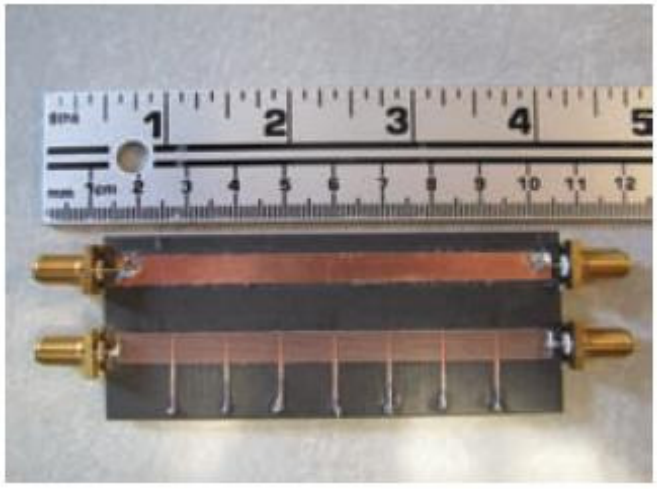

Figure 31. Photograph of the Manufactured Seven Unit Cell RH-/CRLH Coupled Transmission Lines for Case 3.

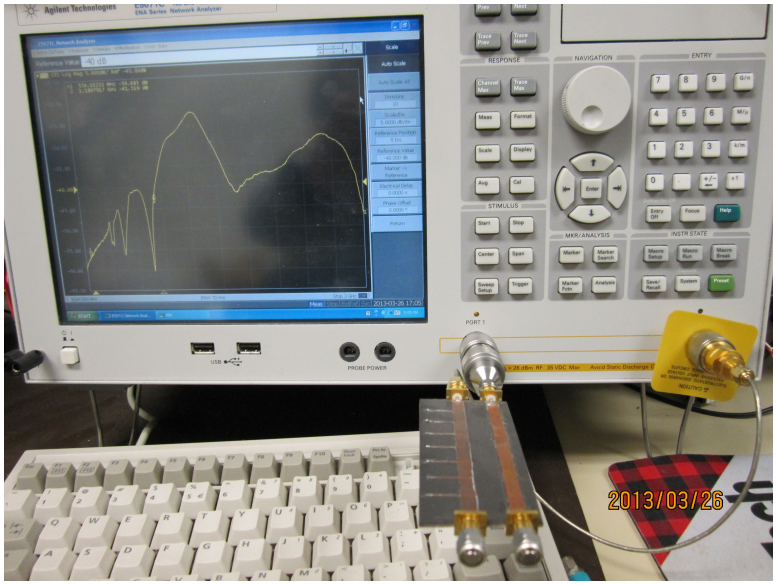

Figure 32. Observing the Performance of the RH- and CLRH Board for the Near-End Coupling.

4.3. Effects of the Left-Handed Components on Noise Voltages

In this section the effects of the left-handed components on noise voltages that are induced on the CRLH-TL will be explored using the analytical expressions (3.8), (3.28) and (3.30). We will see how varying the values of the left-handed parameters L_L and C_L in the CRLH-TL can be used to reduce the noise voltage coupling between the RH-and CRLH-TL. This will be shown here for near-end coupling for different resistance values. For that purpose, the analytical expression obtained in equation (3.30) will be evaluated for various values of L_L and C_L under the condition where $R_L = R_{NE} = R_{FE}$.

4.3.1. Effect of the Component L_L

To demonstrate the effect of L_L on individual near-end inductive and capacitive coupling, V_{NE}^{IND} and V_{NE}^{CAP} will be shown first which is then followed by its overall effect on the total coupling V_{NE}^{TOT}. This will be observed for different values for R_L, R_{NE} and R_{FE} to ensure both capacitive and inductive coupling.

Initially the resistance values were chosen to be $R_L = R_{NE} = R_{FE} = 2\ \Omega$ which would define the case of inductively dominant coupling and satisfy the inequalities mentioned in [17] for inductively coupled transmission lines at low frequencies. In order to evaluate this the source was varied over a range of 0.5 to 3.0 GHz for various values of L_L, with C_L fixed at 0.3 pF. The evaluation

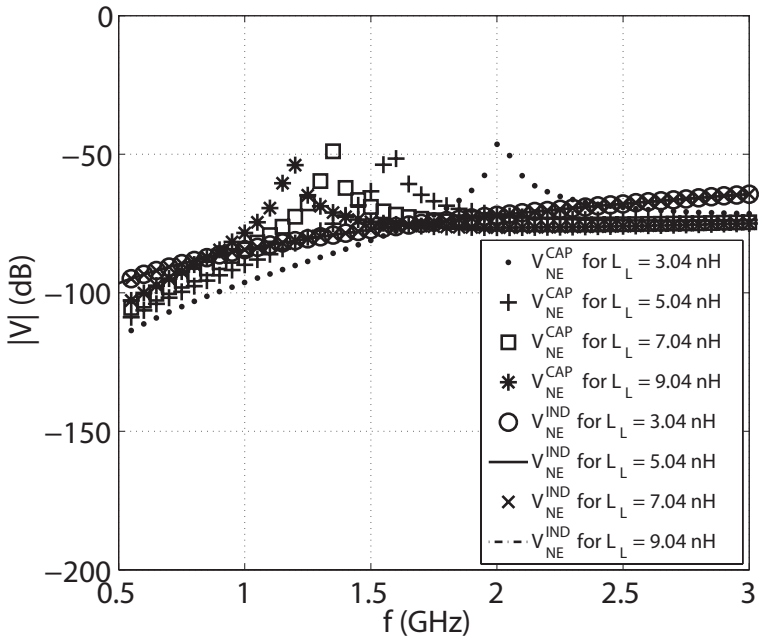

Figure 33. Near-End Voltage due to Inductive and Capacitive Coupling for Various Values of L_L with R_L = 2 Ω.

was carried out using equations (3.8) and (3.28) to compute the near-end voltages for inductive and capacitive coupling, respectively. Also, the total near-end coupling was computed using equation (3.30). The computed results for the near-end inductive and capacitive coupling can be seen in Figure 33 with the total near-end coupling in Figure 34 for the various values of L_L. The results in Figure 33 show that inductive coupling is dominant at the lower frequency indicating the low R_L assumption to support inductive coupling is accurate. The results in Figure 34 also show that for lower values of L_L near-end coupling voltage can be reduced at lower frequencies.

Next, the value of R_L was defined to be 34 Ω and 200 Ω. A value of R_L = 34 Ω would define the case of significant inductive and capacitive coupling both, and a value of R_L = 200 Ω will support a dominant capacitive coupling. For R_L = 34 Ω and R_L = 200 Ω the near-end voltages due to inductive and capacitive coupling are shown in Figures 35 and 37, respectively, with total coupling shown in Figures 36 and 38, respectively. The results obtained for R_L = 34 Ω in Figure 35 are more distinct as compared to the results in Figure 33 indicating a presence of more capacitive coupling. Finally, for R_L = 200 Ω, the results obtained in Figure 37 indicates the presence of dominant capacitive coupling.

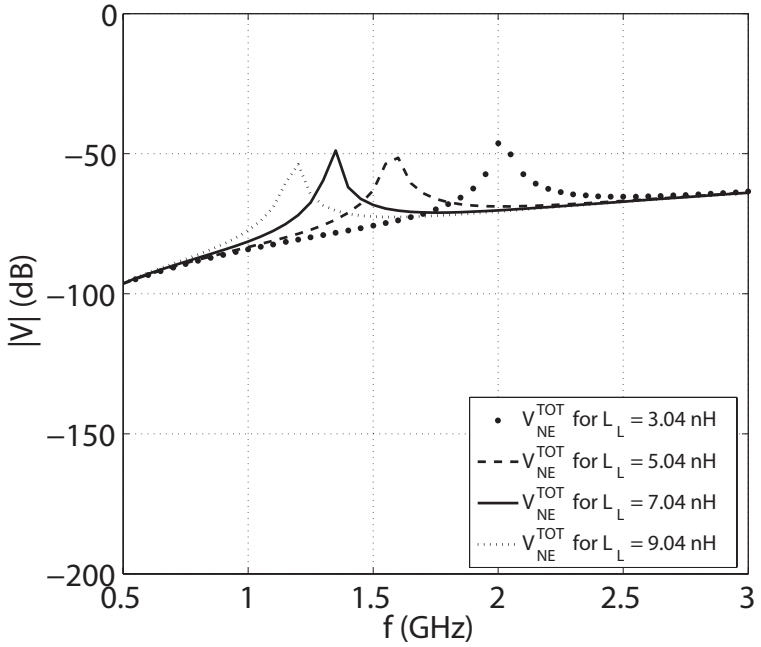

Figure 34. Total Near-End Voltage for Various Values of L_L with $R_L = 2\ \Omega$.

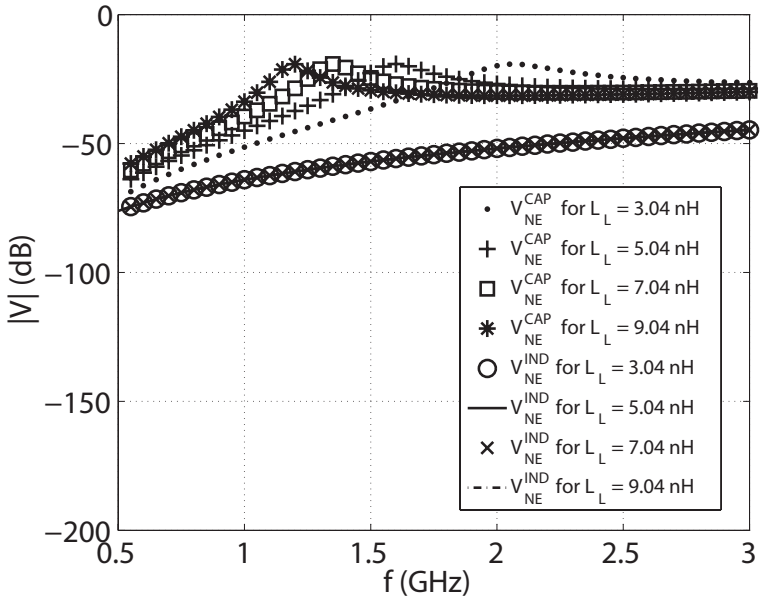

Figure 35. Near-End Voltage due to Inductive and Capacitive Coupling for Various Values of L_L with $R_L = 34\ \Omega$.

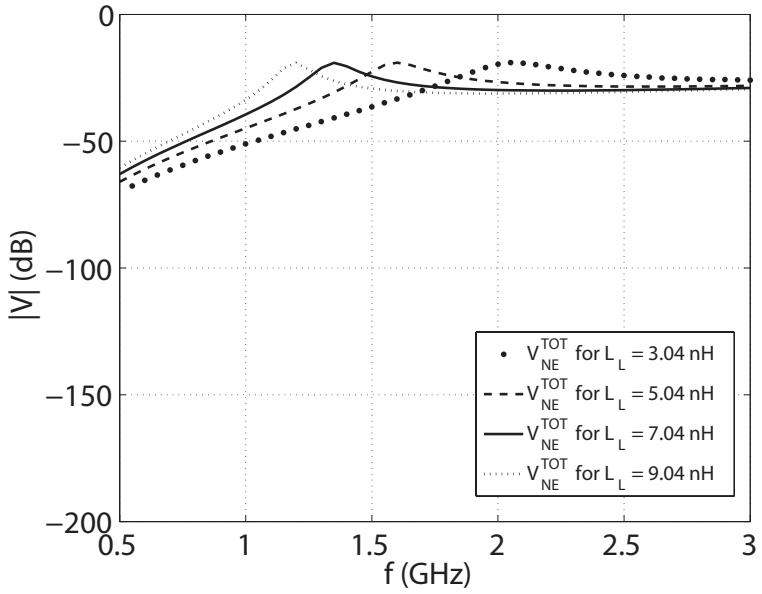

Figure 36. Total Near-End Voltage for Various Values of L_L with $R_L = 34\ \Omega$.

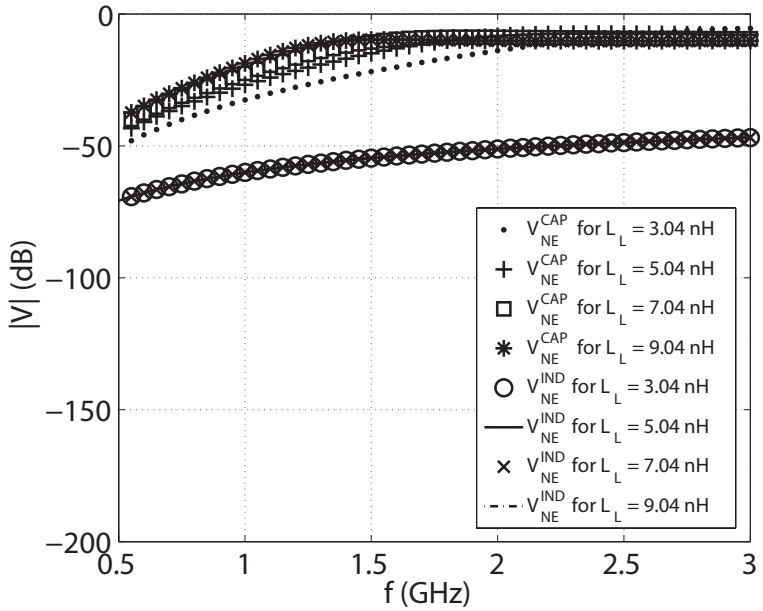

Figure 37. Near-End Voltage due to Inductive and Capacitive Coupling for Various Values of L_L with $R_L = 200\ \Omega$.

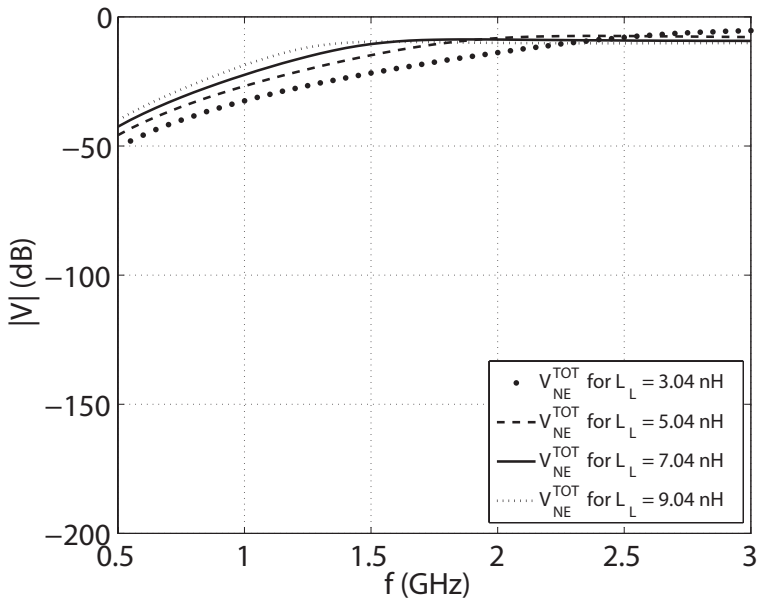

Figure 38. Total Near-End Voltage for Various Values of L_L with $R_L = 200\ \Omega$.

4.3.2. Effect of the Component C_L

Similarly, the effect of C_L on the near-end coupling will be investigated for various value of C_L. This will again be performed for the same values of R_L, R_{NE} and R_{FE}, where $R_L = R_{NE} = R_{FE}$. To begin with we again vary the source over the range 0.5 to 3.0 GHz with L_L fixed at 3.04 nH. The same equations corresponding to (3.8) and (3.28) will be used to evaluate the near-end inductive and capacitive coupling voltages, followed by the total coupling voltage using equation (3.30). For $R_L = 2\ \Omega$, the near-end inductive and capacitive coupling results can be seen in Figure 39 with the total coupling shown in Figure 40. The results obtained in Figure 39 clearly indicate that again the inductive coupling is dominant. Similar observation can be made when L_L was the varying parameter for $R_L = 2\ \Omega$. Also, the results obtained in Figure 40 for the total coupling indicates that the near-end voltages can again be reduced by defining lower values of C_L. The results for other values of $R_L = 34\ \Omega$ and $200\ \Omega$ are also shown in Figures 41, 42, 43 and 44 which again follows the similar trend as was observed for the effects of L_L.

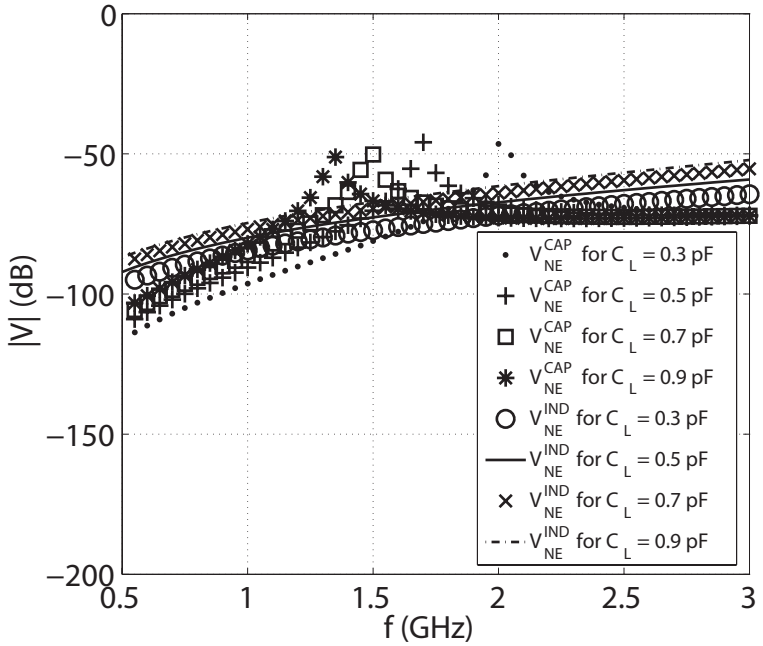

Figure 39. Near-End Voltage due to Inductive and Capacitive Coupling for Various Values of C_L with R_L = 2 Ω.

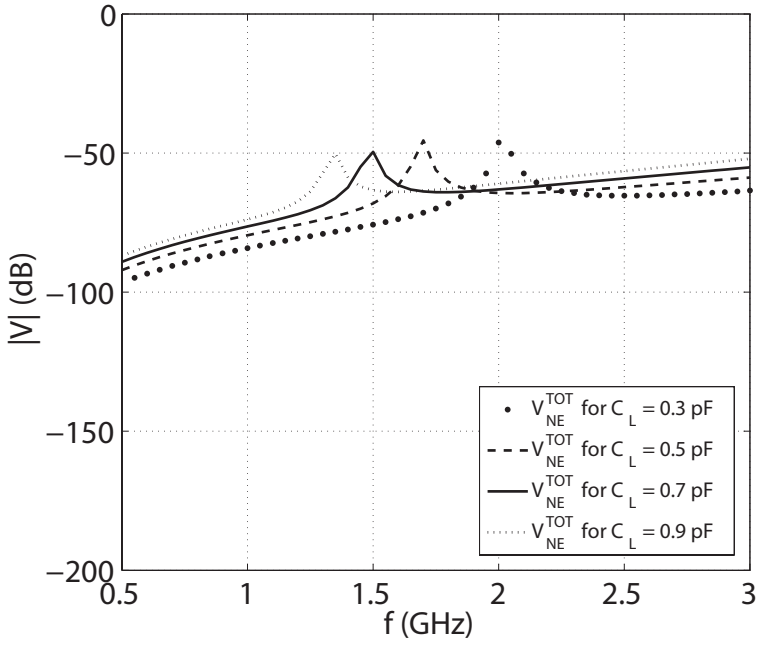

Figure 40. Total Near-End Voltage for Various Values of C_L with R_L = 2 Ω.

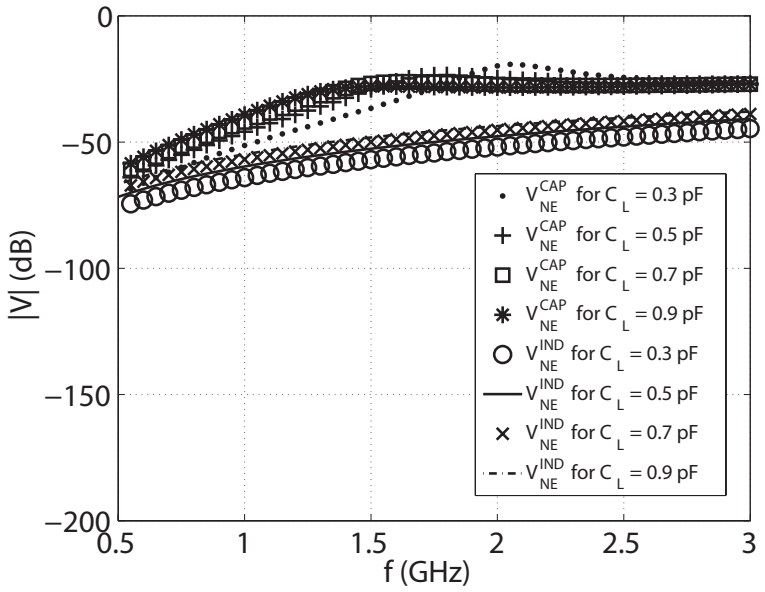

Figure 41. Near-End Voltage due to Inductive and Capacitive Coupling for Various Values of C_L with R_L = 34 Ω.

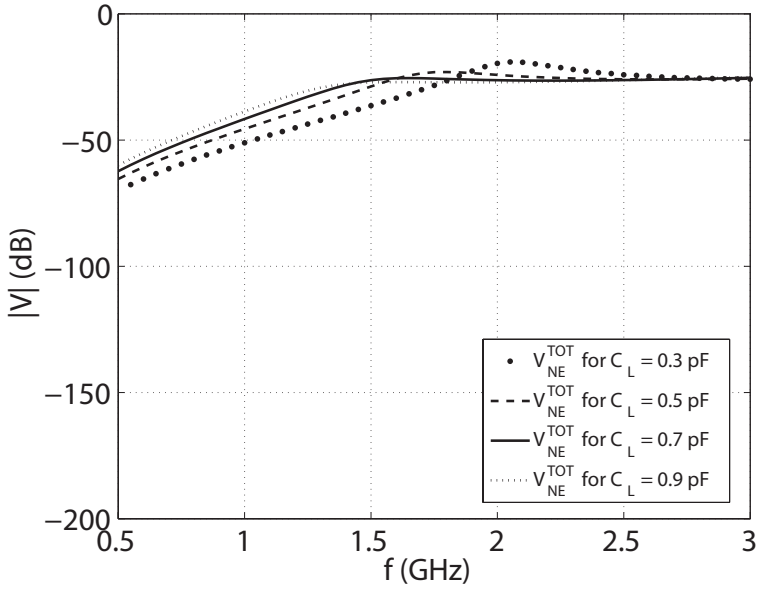

Figure 42. Total Near-end Voltage for Various Values of C_L with R_L = 34 Ω.

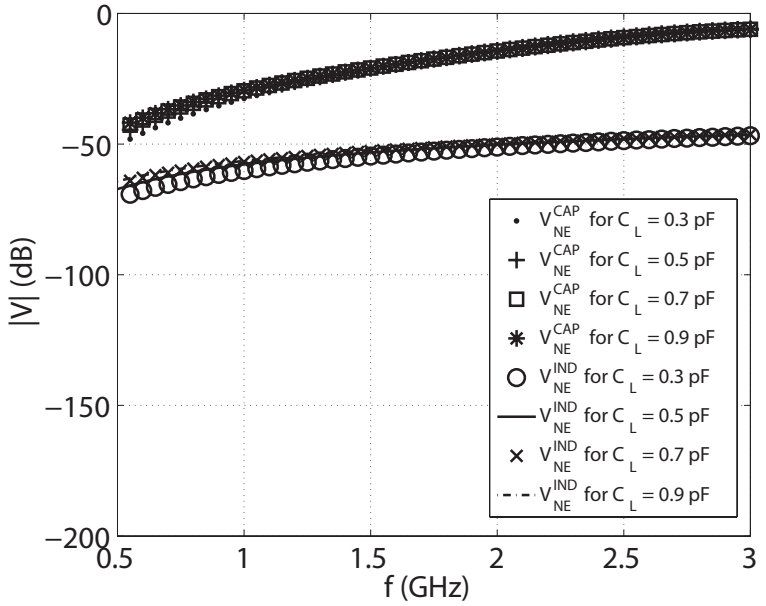

Figure 43. Near-End Voltage due to Inductive and Capacitive Coupling for Various Values of C_L with R_L = 200 Ω.

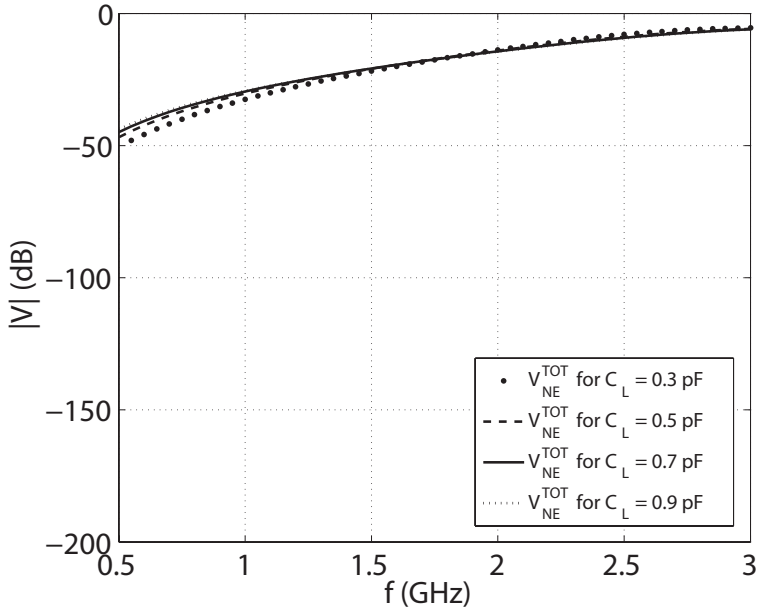

Figure 44. Total Near-End Voltage for Various Values of C_L with R_L = 200 Ω.

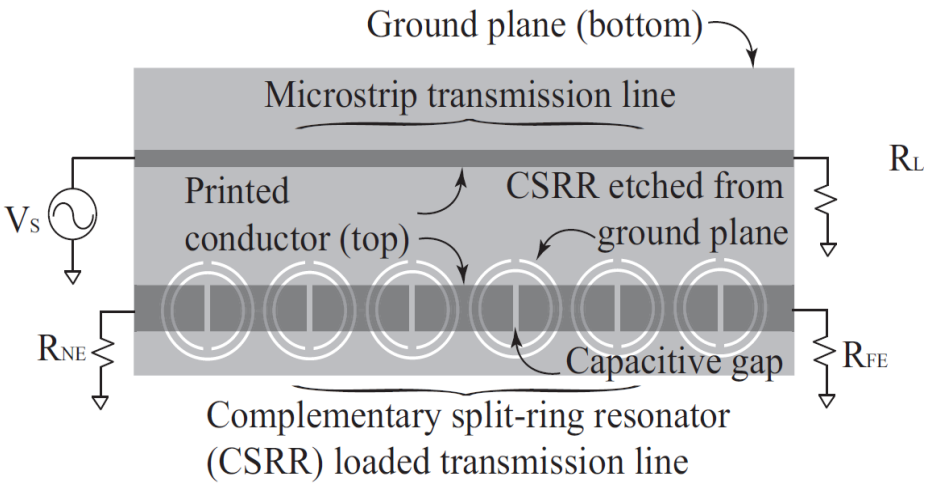

Figure 45. Coupled Conventional Right-Handed and Complementary Split Ring Resonator Transmission Lines.

4.4. 7 Unit Cells of the Coupled RH- and CSRR Transmission Lines

For the validation of the equivalent circuit model of the coupled RH- and CSRR-TLs the 7 unit-cell problem shown in Figure 45 was simulated in Momentum, manufactured and then experimentally tested. After validation its single unit circuit equivalent was then used to explore the noise voltages being induced on the CSRR-TL from the conventional microstrip transmission line.

4.4.1. Layout

The Layout of the 7 unit cells of coupled RH- and CSRR-TLs corresponds to the drawing shown in Figure 24 which shows a RH-TL and a microstrip TL loaded with capacitive gaps and resonating ring structures at periodic intervals.

4.4.2. Simulation and Measurement Results

Initially, the single unit-cell in Figure 19 of the RH- and CSRR-TLs was designed in Momentum [20]. The dimensions for the design correspond to the notation used in Figure 19 which are as follows: a = 3.85 mm, b = 0.28 mm, c = 0.18 mm, d = 0.328 mm, e = 0.328 mm, g = 0.3 mm, Δp = 11.82 mm, r = 4.8 mm, s = 10.0 mm and w = 1.15 mm. The notations Δp and s corresponds

Table 3. Extracted Equivalent Circuit Values for the Coupled RH- and CSRR-TL Unit Cells.

$L_R(nH)$	$C_L(pF)$	$L_L(nH)$	$C_R(pF)$	$L_G(nH)$	$C_G(pF)$	$L_{GR}(nH)$	$C_{GR}(pF)$	$C_c(pF)$
4.96	1.27	3.22	4.01	9.875	1.968	0.11036	0.06786	19.58

to the length of the RH- and CSSR-TL unit cell and the spacing between them, respectively. After carrying out the simulation of the RH- and CSRR-TL unit cell in Momentum, the S-parameters were used in the extraction of the equivalent circuit model of the unit cell. This was again done using the matrix method as applied in the case of the coupled RH- and CRLH-TLs where the parameters were extracted at the transition frequency f_0 of the RH-/LH band. The extracted values are shown in Table 3.

After determining the equivalent circuit parameters of the design, the next step was to model the coupled unit cells in the ADS simulation tool Designer in order to determine the accuracy. This was accomplished by cascading 7 cells of the unit circuit in Figure 20 to model the layout in Figure 45. An image of the circuit being simulated in Designer is shown in Figure 46. The simulation result obtained for the layout shows good agreement with its equivalent circuit result which can be seen in Figure 47. Finally, the coupled transmission lines were then manufactured on a 1.27 mm thick Rogers RT/duroid 6010.2LM ($\epsilon_r = 10.2$, $\tan\delta = 0.0023$) [21] substrate as shown in Figures 48 and 49. The picture in Figure 48 represents the top conducting layer of the dielectric substrate comprising of a conventional microstrip TL coupled to the left-handed TL loaded with series capacitive gaps. The picture in Figure 49 represents the bottom ground layer of the dielectric substrate comprising of complementary split ring resonators (CSRRs) loaded to the left-handed transmission line on the top with series capacitive gaps. A picture of the device under test can be seen in Figure 50 for near-end coupling using an Agilent ENA series network analyzer The ports not being used are terminated with 50 Ω load. The measurements are shown in Figure 47.

The results obtained for the design in terms of the equivalent circuit, the full-wave simulation and the measurement all shows agreement among them stating that the equivalent circuit in Figure 20 is a good model to represent the coupling between RH- and CSRR-TL.

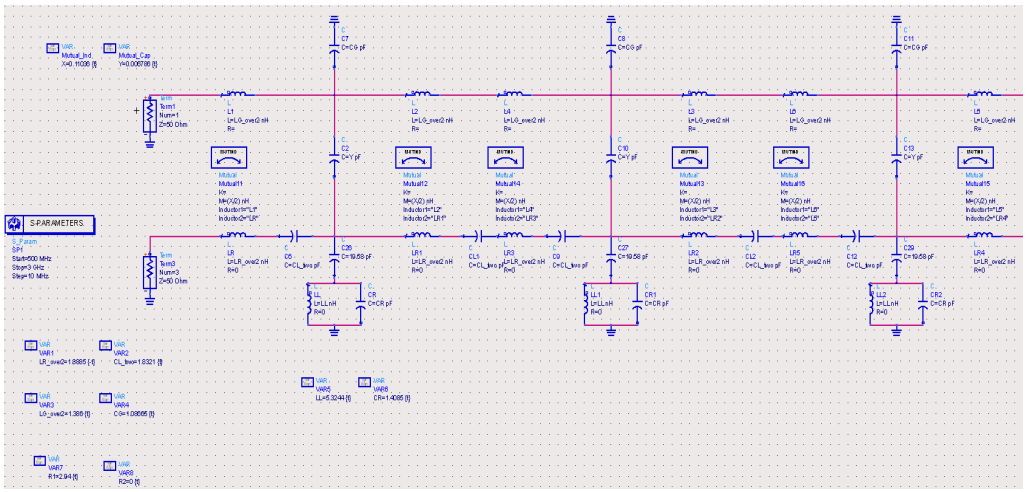

Figure 46. Circuit Equivalent of the Seven Unit Cell Coupled RH- and CRLH-TLs in Designer.

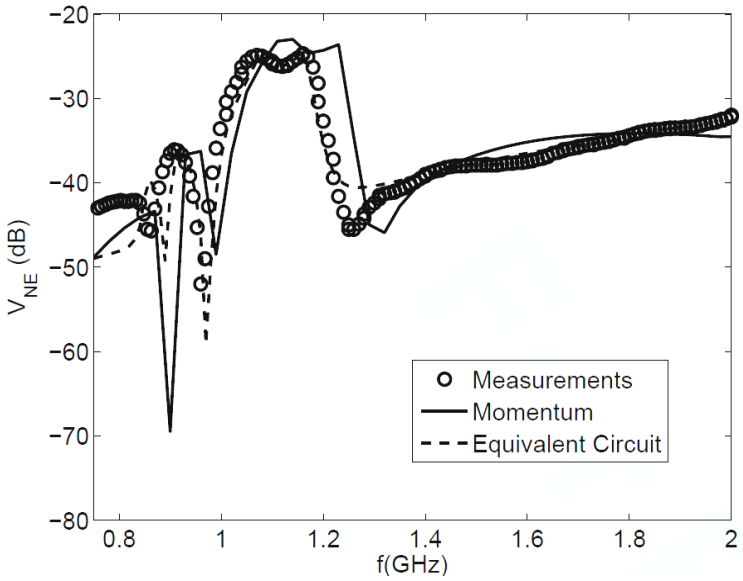

Figure 47. Measurement and Simulation Results of the Seven Unit Cell Prototype Board.

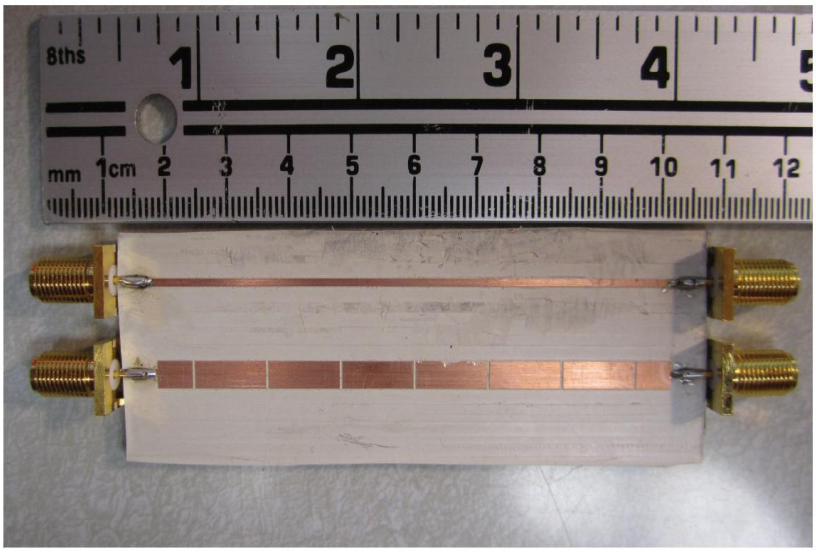

Figure 48. Top View of the Manufactured Seven Unit Cell RH-/CSRR Coupled Transmission Lines.

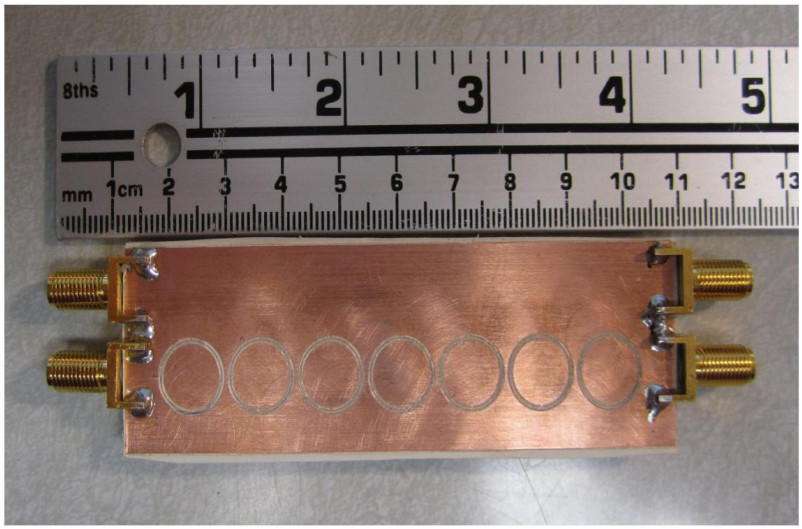

Figure 49. Bottom View of the Manufactured Seven Unit Cell RH-/CSRR Coupled Transmission Lines.

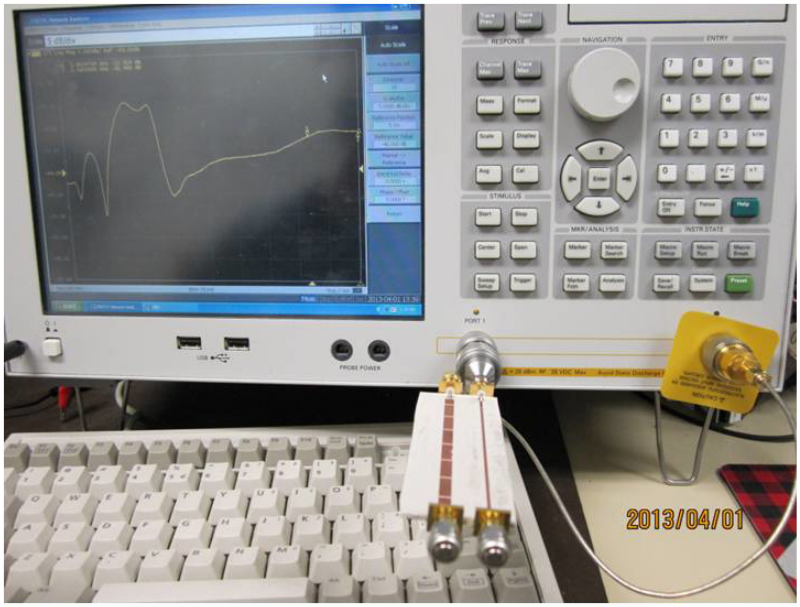

Figure 50. Observing the Performance of the RH- and CSRR Board for the Near-End Coupling.

CHAPTER 5. DESIGN TRADE-OFFS, GUIDELINES AND DISCUSSION

5.1. Introduction

In this chapter, we will be looking at the design trade-offs and spacing guidelines for the RH- and CRLH-TL, followed by spacing guidelines for the RH- and CSRR-TL. Furthermore, we will compare the results to the coupling to microstrip TLs. Finally, we will determine the left-handed structure that will generate the least amount of crosstalk or noise voltage coupling on printed circuit boards.

5.2. The Coupled Voltages - L_L, C_L Relationship

So far, the results in Figures 34, 36, 38, 40, 42 and 44 showed that the near-end voltages can be reduced by reducing the values of left-handed components L_L and C_L. This can be demonstrated in two ways: by looking at the equivalent general coupling circuit of the RH- and CRLH-TLs shown in Figure 13 and from the analytical expressions obtained in (3.30) and (3.31). First if we consider the equivalent circuit by reducing the value of L_L, we will notice that the result would lower the parallel shunt impedance comprising of L_L and C_R. This would increase the current through the shunt impedance. Thus, current flowing through R_{NE} and R_{FE} would decrease, which would therefore reduce the unwanted coupled voltages. Similarly, if we reduce the value of C_L, then the impedance of the left-handed capacitance would increase. This would once again reduce the current through R_{NE} and R_{FE}, which also reduces the unwanted coupled voltages.

This relationship between coupled voltages and L_L, C_L can also be illustrated using the analytical expressions in (3.30) and (3.30). If we decrease the value of L_L, the parallel impedance Z_P in (3.5) reduces. This then causes the impedance Z_{eq} in (3.2) to increase which in-turns reduces the capacitively coupled voltage V_c in (3.1). Similarly, if we decrease the value of C_L, then the values of the near- and far-end impedance expressions in (3.3) and (3.4), respectively, increases. This then leads to a decrease in capacitively coupled voltages expressed in (3.8) and (3.9). A similar observation can be drawn for the inductively coupled voltages in (3.28) and (3.29).

5.3. Trade-Offs between Reduced Coupled Voltages and the Propagation Characteristics of the CRLH-TL

While designing a CRLH-TL, there are certain propagation characteristics of the line that should be considered. In particular, the cut-off frequency for the left-handed propagation and the transition frequency from the left-handed to the right-handed region. The cut-off frequency here,

Table 4. Cut-off and Transition Frequencies for the CRLH-TL for Measurement Cases 1, 2 and 3.

Case	$f_{CL}(GHz)$	$f_0(GHz)$
1	1.16	2.47
2	0.879	2.14
3	1.05	2.35

denoted as f_{CL}, represents the lowest frequency for which the CRLH-TL will support left-handed propagation. Whereas the transition frequency denoted as f_0 represents the frequency at which the CRLH-TL transitions from supporting left-handed propagation to right-handed propagation. For all the prior discussed cases, $f_{CL} < f_0$. Generally, if we were to compute the lower cut-off for the left-handed propagation and the transition frequency of a CRLH-TL then it can be computed using [7] as follows:

$$f_{CL} = f_0\sqrt{\frac{P_1 - P_2}{2}} \tag{5.1}$$

where

$$P_1 = [K + (2/\omega_L)^2]\omega_0^2, \tag{5.2}$$

$$P_2 = \sqrt{P_1^2 - 4}, \tag{5.3}$$

$$f_0 = \frac{1}{2\Pi\sqrt[4]{L_R C_R L_L C_L}}, \tag{5.4}$$

$$f_L = \frac{1}{2\Pi\sqrt{L_L C_L}} \tag{5.5}$$

and K = $L_R C_L + L_L C_R$. To determine these cut-off and transition frequencies, the extracted parameters in Table 2 of the coupled transmission lines shown in Figures 29, 30 and 31 are used in equations (5.1) through (5.5) for cases 1, 2 and 3. The evaluated lower cut-off and the transition frequencies are shown in Table 4. If we closely examine the evaluated values of all the cases while taking case 2 as a referenced then, it can be observed that by reducing the length of the stub inductor in case 1, the lower left-handed propagating cut-off frequency has increased. A similar observation can also be made for case 3 where also by reducing the gap capacitance between the interdigitated fingers of the structure results in an increased lower left-handed cut-off frequency. These evaluated values of f_{CL} for cases 1, 2 and 3 are also labeled in Figures 26, 27 and 28, respectively, for comparison. Similarly, the transition frequency f_0 from the left-handed to right-handed propagating region was also evaluated using equation (5.4) for cases 1, 2 and 3. These values are shown in Table 4 and in Figures 26, 27 and 28 for comparison. A similar trend of increasing values of f_0 can be

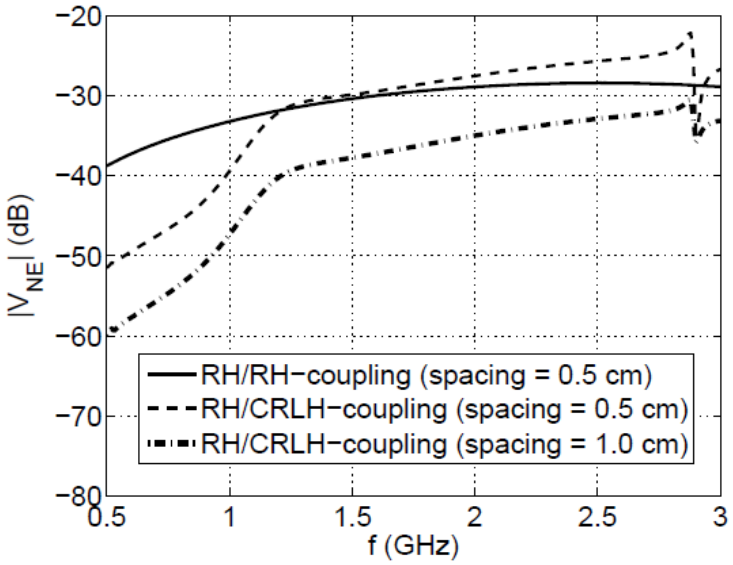

Figure 51. Total Near-End Voltage for a Spacing of s = 0.5 cm and 1.0 cm.

observed as in the case of f_{CL} for lower values of L_L and C_L. Therefore, in summary it can be concluded that decreasing the values of L_L and C_L definitely serves our purpose of reducing the near- and far-end coupled voltages as seen in Figures 34, 36, 38, 40, 42, and 44 which can prove to be a useful alternative to conventional shielding. However, the consequences or the trade-offs, of lowering these left-handed parameters of the CRLH-TL for reducing the noise voltages are that we might disturb the lower cut-off of the left-handed operating band and the transition frequency by increasing their values.

5.4. Spacing Design Guidelines for the CRLH-TL

Finally, the spacing guidelines have been investigated between RH- and CRLH-TLs and compared to the coupling between two conventional microstrip RH-TLs. This investigation was performed using a similar design of the RH and symmetric CRLH-TL unit cells shown in Figure 12 and then compared to a pair of coupled RH-TLs(or microstrip TLs) with the same unit cell length and spacing. It was carried out in ADS Momentum, first for a same spacing of s = 0.5 cm for both the pairs of TLs and then for a spacing of s = 1 cm for only RH- and CRLH-TLs in order to observe the change and the difference in level of coupling between different pairs of TLs. The dimensions adopted for each unit cell (both RH-TL and CRLH-TL) for these simulations were the

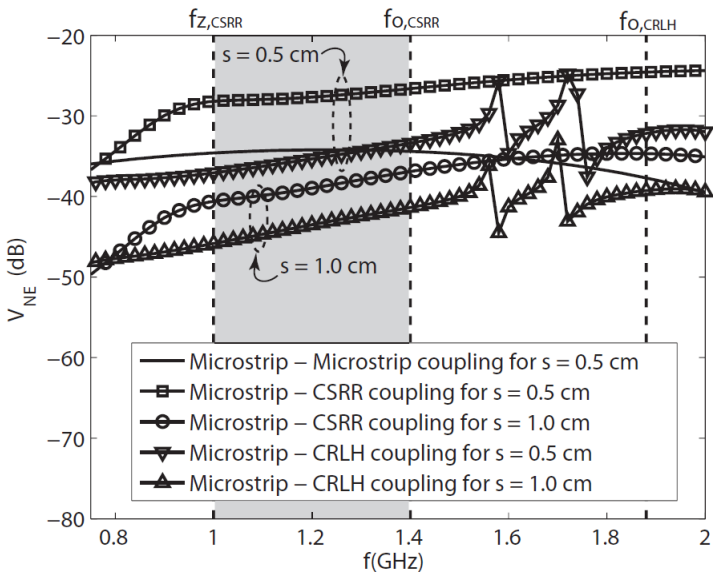

Figure 52. Comparing the Coupling to the CSRR-Loaded Transmission Lines to the Coupling to a Microstrip (Right-Handed) and the CRLH-TLs Reported in [18] for Various Spacing Values s.

same as defined in case 2 shown in Figure 30. The simulation results for near-end voltages can be seen in Figure 51. From the results it can be clearly seen that for a spacing of s = 0.5 cm the near-end voltages induced onto the CRLH-TL from the conventional RH-TL seems to increase over the voltages induced onto the RH-TL at 1.25 GHz. Now, if we compare this frequency to the set of frequency values f_{CL} and f_0 obtained in Table 4 for case 2 then, it clearly defines that this transition takes place in the left-handed propagating band. Also, it can be noticed that for the frequencies above the transition frequency f_0, the near-end voltages induced onto the CRLH-TL are larger than the near-end voltages induced onto the RH-TL from the conventional TL.

Next, when a gap separation of s = 1 cm was applied between the RH- and CRLH-TL then it resulted in near-end voltages on the CRLH-TL that were less than the near-end voltages on the RH-TL. This illustrates that spacing should be carefully taken into account while designing a CRLH-TL in close proximity of the conventional RH-TL.

5.5. Spacing Design Guidelines for the CSRR-TL

In order to examine the spacing requirements for RH- and CSSR-TLs, a similar procedure to that used for the CRLH-TL was followed. In particular, the coupled unit cell of a RH- and CSRR-TL

shown in Figure 19 was simulated in ADS Momentum. This was again carried out for spacings of s = 0.5 cm and 1.0 cm and compared to the coupling between two conventional microstrip RH-TLs. The dimensions adopted for each unit cell (both RH-TL and CSRR-TL) for the simulations were the same, with the notations used in Figure 19 and values mentioned under section 4.4.2. The results for these simulations are shown in Figure 52. For further comparison, the coupling between the RH- and CRLH-TL unit cells shown in Figure 12 was also simulated and are shown in Figure 52.

In all by looking at the results obtained in Figure 52 several comments can be made. First, for a spacing of s = 0.5 cm, the near-end noise voltages coupled to the CSRR-TL are approximately 10 dB higher than the near-end voltages coupled to the RH-TL over the desired left-handed band. Next, for an increased spacing of s = 1.0 cm, they are lower than the near-end voltages coupled to the RH-TL for same spacing of s = 0.5 cm over the same band of interest. This again signifies that a larger spacing should be considered while designing a CSRR loaded microstrip line in close proximity of the conventional RH-TL.

For the left-handed transmission lines such as the CRLH- and CSRR-TL, an important feature is the left-handed propagation band. The left-handed propagating bands for the CRLH- and CSRR-TL designs depicted in Figures 12 and 19 can be seen in Figure 52. For the CSRR-TL the left-handed propagating band is between $f_{Z,CSRR}$ and $f_{0,CSRR}$ and the left-handed propagating band for the CRLH-TL is below $f_{0,CRLH}$. The shaded region represents the band that is common to both the CSRR- and CRLH-TLs. A fair comparison on the level of noise voltages being coupled to each TL can be made over this common band. If we closely observe then for both spacing values of s = 0.5 cm and 1.0 cm the noise voltages coupled to the CSRR-TL are approximately 10 dB higher than the noise voltages being coupled to the CRLH-TL. Therefore, from this observation it can be inferred that a larger spacing is required for designing a CSRR-TL next to a conventional microstrip TL, which thus proves the CRLH-TLs may be more useful for compact electronics.

CHAPTER 6. CONCLUSION

Throughout this work the coupling between a conventional microstrip transmission line and metamaterial inspired transmission lines has been studied and analyzed from an EMC point-of-view. In particular, the coupling between a conventional microstrip and a CRLH-transmission line and the coupling between a conventional microstrip and a CSRR loaded transmission line has been presented and discussed. For both of the coupling problems, new analytical expressions for computing the near- and far-end coupling noise voltages were derived. These newly derived expressions have been successfully validated with the full-wave simulation tool Momentum, circuit computations using Designer and measurements. The analytical expressions have also been used for studying the noise voltages on the CRLH-TL. It has been shown that decreasing the values of L_L and C_L along the CRLH-TL could be an alternative solution to conventional shielding. However, there are certain trade-offs between reducing the coupled noise voltages and the left-handed propagation characteristics. Furthermore, spacing design guidelines have been proposed using Momentum to determine the amount of noise voltage being coupled to a CRLH-TL, CSRR-TL and a conventional microstrip TL. It was determined that the CSRR-TL had approximately 10 dB higher coupled noise voltages than the CRLH-TL for the same spacings. These higher voltages are due to the edges of the CSRRs etched from the ground plane that are not placed directly below the the top conducting layer. Therefore, the CSRR-TLs require almost twice the amount of spacing than the CRLH-TLs to have approximately same noise voltages.

Future research could be done to further explore the coupling problem between two CLRH-TLs because of the smaller spacing requirements which could thus be beneficial for compact RF circuitry which is currently moving toward more miniaturized electronics. This could be one advantage of using it over CSSR-TLs which require more spacing for lower noise voltage coupling.

REFERENCES

[1] C. Caloz and T. Itoh, "Electromagnetic Metamaterials: Transmission Line Theory and Microwave Applications," John Wiley and Sons, Inc., Hoboken, NJ, 2006, pp. 86-246.

[2] S. Simion, R. Marcelli, G. Bartolucci, F. Craciunoiu, A. Lucibello, G. D. Angelis, A. A. Muller, A. C. Bunea and G. I. Sajin, "Composite Right/Left Handed (CRLH) based devices for microwave applications," *Advanced Microwave and Millimeter Wave Technologies: Semiconductor Devices, Circuits and Systems*, In Tech Publishing Company, Inc., 2010.

[3] M. Gil, J. Bonache, I. Gil, J. G. Garcia and F. Martin, "On the tranmission properties of left-handed microstrip lines implemented by complementary split rings resonators," *International Journal of Numerical Modelling: Electronic Networks, Devices and Fields*, vol. 19, pp. 87-103, 2006.

[4] F. Falcone, T. Lopetegi, J.D. Baena, J. Bonache, R. Marques, F. Martin and M. Sorolla, "Babinet principle applied to the design of metasurfaces and metamaterials," *Physics Review Letters*, vol. 93, 2004.

[5] C. Caloz and T. Itoh, "A novel mixed conventional microstrip and composite right/left-handed backward-wave directional coupler with broadband and tight coupling characteristics," *IEEE Microw. Guided Wave Lett.*, vol. 14, no. 1, pp. 31-33, Jan. 2004.

[6] B. D. Braaten, S. Roy, I. Ullah, S. Nariyal, B. Ijaz, M. M. Masud, S. A. Naqvi and A. Iftikhar, "A cascaded Reconfigurable RH/CRLH-Zero-Phase Microstrip Transmission Line Unit," *Proceedings of the IEEE International Conference on Wireless Information Technology and Systems, Maui, Hawaii*, Nov. 11th - 16th, 2012.

[7] C. Caloz and T. Itoh, "Metamaterials for High-Frequency Electronics," *Proceedings of the IEEE.*, vol. 93, no. 10, Oct. 2005.

[8] A. Sanada, C. Caloz and T. Itoh, "Novel zeroth-order resonance in composite right/left-handed transmission line resonator," *Proceedings of the Asia-Pacific Microwave Conference,* pp.1588-1591, Nov. 2003.

[9] S. Otto, A. Rennings, C. Caloz, P. Waldow and T. Itoh, "Composite right/left-handed λ-resonator ring antenna for dual-frequency operation," *IEEE Antennas and propagation society Internation symposium,* pp.684-687, vol. 1A, Jul. 2005.

[10] C. Caloz, "Metamaterial dispersion engineering concepts and applications," *Proceedings of the IEEE,* vol. 99, no. 10, May 2011.

[11] A. Sanada, C. Caloz and T. Itoh, "Characteristics of the composite right/left-handed transmission lines," *IEEE Microw. and Wireless Compon. Lett.,* vol. 14, no. 2, Feb. 2004.

[12] R. Marques, F. Martin and M. Sorolla, *Metamaterials with Negative Parameters: Theory, Design and Microwave Applications,* John Wiley and Sons Inc., Hoboken NJ, 2008.

[13] J. Bonache, M. Gil, I. Gil, J. Gracia-Garcia and F. Martin, "On the Electrical Characteristics of Complementary Metamaterials Resonators," *IEEE Microwave and Wireless Components Letters.*, vol. 16, no. 10, Jan. 2006.

[14] N. Engheta and R. W. Ziolkowski, *Metamaterials: Physics and Engineering Explorations,* John Wiley and Sons Inc., Hoboken NJ, 2006.

[15] F. Capolino (Ed.), *Metamaterials Handbook: Applications of Metamaterials,* CRC Press, Boca Raton FL, 2009.

[16] G. V. Eleftheriades and K. G. Balmain, *Negative-Refraction Metamaterials: Fundamental Principles and Applications,* John Wiley and Sons Inc., Hoboken NJ, 2005.

[17] C. Paul, "Intoduction to Electromagnetic Compatibility Electromagnetic," John Wiley and Sons, Inc., Hoboken, NJ, 2006, pp. 599-601.

[18] I. Irfanullah, S. Nariyal, S. Roy, M. M. Masud, B. Ijaz and B. D. Braaten, "Analysis of the noise voltage coupling (crosstalk) between right-handed and composite right/left-handed (CRLH) transmission lines on printed circuit boards," *IEEE Transactions on Electromagnetic Compatibility*, vol. PP, Issue:99, Dec. 2012.

[19] Matlab, (2010) [online] www.mathworks.com.

[20] Advanced Design System (ADS) by Agilent Technologies, (2012) [online] www.agilent.com.

[21] Rogers Corporation, (2012) [online] www.rogerscorp.com.

APPENDIX A. MATLAB CODE : RH-CRLH COUPLING

The following file

`RH_CRLH_Coupling.m`.

was used to determine the near-end and far-end capacitive, inductive and total coupling for RH- and CRLH-TL unit cell for different values of load terminations which corresponds to the Figures shown in 16, 17 and 18.

```
%%%%%%%%%%%%%%%%%%%%%%%%%%%% RH_CRLH_COUPLING FILE %%%%%%%%%%%%%%%%%%%%%%%%%%%%
%%%%%%%%%%%%%%%%%%%%%%%%%%%%%%%%%%%%%%%%%%%%%%%%%%%%%%%%%%%%%%%%%%%%%%%%%%%%%%%
clc
clear all
close all
f = 100e6:10e6:3e9;
w=2*pi*f;
Vs = 1;
Rs = 50;
Cg = .33e-12;
Cgr = .33e-12;
Lr = 1.1e-9;
Rl = 200;
Rne = 200;
Rfe = 200;
Cr = .45e-12;
Ll = 3.04e-9;
Cl = 1.3e-12;
Lgr = .13e-9;

Zlr = j*w*Lr/2;
Zcr = -j./(w*Cr);
Zll = j*w*Ll;
Zcgr = -j./(w*Cgr);
Zcg = -j./(w*Cg);
Zcl = -j./(2*w*Cl);
Zl = Zcr.*Zll./(Zcr+Zll);
Zdne = Zcl+Zlr+Rne+Zl;
Zdfe = Zcl+Zlr+Rfe+Zl;
Zlgr = j*w*Lgr/2;
Zne = Zcl+Zlr+Rne;
Zfe = Zcl+Zlr+Rfe;

%%%%%%%%%%%%%%%%%%%%%%Capacitive Coupling%%%%%%%%%%%%%%%%%%%%%%%%%
figure
Vin = Vs*Rl/(Rl+Rs);
Zeq = Zne.*Zfe.*Zl./(Zfe.*Zl+Zne.*Zl+Zne.*Zfe);
Vn = Vin*Zeq./(Zeq+Zcgr);
Vne_cap = Vn*Rne./(Rne+Zcl+Zlr);
Vfe_cap = Vn*Rfe./(Rfe+Zcl+Zlr);
semilogx(f,20*log10(abs(Vne_cap)),'.',f,20*log10(abs(Vfe_cap)),'-')
xlabel('f (Hz)')
ylabel('|V| (dB)')
legend('V_{ne}','V_{fe}')
title('Capacitive Coupling')
axis([100e6 3e9 -200 0])
grid on

%%%%%%%%%%%%%%%%%%%%%%Inductive Coupling%%%%%%%%%%%%%%%%%%%%%%%%%
figure
```

```
Ig = Vs/(Rs+Rl);
I2=Ig.*Zlgr.*(Zl+Zdne)./(Zdfe.*Zdne-Zl.^2);
Vne_ind=Rne*I2;
I1=Ig.*Zlgr.*(Zl+Zdfe)./(Zdfe.*Zdne-Zl.^2);
Vfe_ind=Rfe*I1;
semilogx(f,20*log10(abs(Vne_ind)),'.',f,20*log10(abs(Vfe_ind)),'-')
xlabel('f (Hz)')
ylabel('|V| (dB)')
legend('V_{ne}','V_{fe}')
title('Inductive Coupling')
axis([100e6 3e9 -200 0])
grid on

%%%%%%%%%%%%%%%%Near-end Total coupling %%%%%%%%%%%%%%%%%%%%
figure
Vne=Vne_cap+Vne_ind;
semilogx(f,20*log10(abs(Vne)),'.k',f,20*log10(abs(Vne_ind)),'--k', ...
    f,20*log10(abs(Vne_cap)),'-k')
xlabel('f (Hz)')
ylabel('|V_{NE}| (dB)')
legend('V_{ne}^{TOT}','V_{ne}^{IND}','V_{ne}^{CAP}')
title('Near-End Total Coupling')
axis([100e6 3e9 -200 0])
grid on

%%%%%%%%%%%%%%%%%%Far-end Total Coupling %%%%%%%%%%%%%%%%%%%%
figure
Vfe=Vfe_cap+Vfe_ind;
semilogx(f,20*log10(abs(Vfe)),'.k',f,20*log10(abs(Vfe_ind)),'--k', ...
    f,20*log10(abs(Vfe_cap)),'-k')
xlabel('f (Hz)') ylabel('|V| (dB)')
legend('V_{fe}^{TOT}','V_{fe}^{IND}','V_{fe}^{CAP}') title('Far-End
Total Coupling') axis([100e6 3e9 -200 0]) grid on
grid on
```

APPENDIX B. MATLAB CODE : RH-CRLH COUPLING EFFECTS

The following file

`RH_CRLH_Coupling_Effects.m`.

was used to determine the effects of L_L and C_L on inductive, capacitive and total coupling for different values of load terminations which corresponds to the Figures shown from 33 - 44.

```
%%%%%%%%%%%%%%%%%%%%%%%% RH_CRLH_COUPLING_EFFECTS FILE %%%%%%%%%%%%%%%%%%%%%%%%%%
%%%%%%%%%%%%%%%%%%%%%%%%%%%%%%%%%%%%%%%%%%%%%%%%%%%%%%%%%%%%%%%%%%%%%%%%%%%%%%%%
clc
clear all
close all
f =[10e6:10e6:3e9];
w=2*pi*f;
Vs = 1;
Rs = 50;
Rl = 2;
Rne = 2;
Rfe = 2;
Cg = .33e-12;
Cgr = .33e-12;
Lr = 1.1e-9;
Cr = .45e-12;
Lgr = .13e-9;

%%%%%%%%%%%%%%%%%%%%%%%%%%%%%% Varying values of Ll %%%%%%%%%%%%%%%%%%%%%%%%%%%%%5
% Ll = 3.04e-9;
Ll = 3.04e-9;
Cl = .3e-12;
Zlr = j*w*Lr/2;
Zcr = -j./(w*Cr);
Zll = j*w*Ll;
Zcgr = -j./(w*Cgr);
Zcg = -j./(w*Cg);
Zcl = -j./(2*w*Cl);
Zl = Zcr.*Zll./(Zcr+Zll);
Zdne = Zcl+Zlr+Rne+Zl;
Zdfe = Zcl+Zlr+Rfe+Zl;
Zlgr = j*w*Lgr/2;
Zne = Zcl+Zlr+Rne;
Zfe = Zcl+Zlr+Rfe;

Vin = Vs*Rl/(Rl+Rs);
Zeq = Zne.*Zfe.*Zl./(Zfe.*Zl+Zne.*Zl+Zne.*Zfe);
Vn = Vin*Zeq./(Zeq+Zcgr);
Vne_cap_1 = Vn*Rne./(Rne+Zcl+Zlr);
Vfe_cap_1 = Vn*Rfe./(Rfe+Zcl+Zlr);
Ig = Vs/(Rs+Rl);
I2=Ig.*Zlgr.*(Zl+Zdne)./(Zdfe.*Zdne-Zl.^2);
Vne_ind_1=Rne*I2;
I1=Ig.*Zlgr.*(Zl+Zdfe)./(Zdfe.*Zdne-Zl.^2);
Vfe_ind_1=Rfe*I1;

% Ll = 5.04e-9;
Ll = 5.04e-9;
Zlr = j*w*Lr/2;
Zcr = -j./(w*Cr);
Zll = j*w*Ll;
Zcgr = -j./(w*Cgr);
```

```
Zcg = -j./(w*Cg);
Zcl = -j./(2*w*Cl);
Zl = Zcr.*Zll./(Zcr+Zll);
Zdne = Zcl+Zlr+Rne+Zl;
Zdfe = Zcl+Zlr+Rfe+Zl;
Zlgr = j*w*Lgr/2;
Zne = Zcl+Zlr+Rne;
Zfe = Zcl+Zlr+Rfe;

Vin = Vs*Rl/(Rl+Rs);
Zeq = Zne.*Zfe.*Zl./(Zfe.*Zl+Zne.*Zl+Zne.*Zfe);
Vn = Vin*Zeq./(Zeq+Zcgr);
Vne_cap_2 = Vn*Rne./(Rne+Zcl+Zlr);
Vfe_cap_2 = Vn*Rfe./(Rfe+Zcl+Zlr);
Ig = Vs/(Rs+Rl);
I2=Ig.*Zlgr.*(Zl+Zdne)./(Zdfe.*Zdne-Zl.^2);
Vne_ind_2=Rne*I2;
I1=Ig.*Zlgr.*(Zl+Zdfe)./(Zdfe.*Zdne-Zl.^2);
Vfe_ind_2=Rfe*I1;

% Ll = 7.04e-9;
Ll = 7.04e-9;
Zlr = j*w*Lr/2;
Zcr = -j./(w*Cr);
Zll = j*w*Ll;
Zcgr = -j./(w*Cgr);
Zcg = -j./(w*Cg);
Zcl = -j./(2*w*Cl);
Zl = Zcr.*Zll./(Zcr+Zll);
Zdne = Zcl+Zlr+Rne+Zl;
Zdfe = Zcl+Zlr+Rfe+Zl;
Zlgr = j*w*Lgr/2;
Zne = Zcl+Zlr+Rne;
Zfe = Zcl+Zlr+Rfe;

Vin = Vs*Rl/(Rl+Rs);
Zeq = Zne.*Zfe.*Zl./(Zfe.*Zl+Zne.*Zl+Zne.*Zfe);
Vn = Vin*Zeq./(Zeq+Zcgr);
Vne_cap_3 = Vn*Rne./(Rne+Zcl+Zlr);
Vfe_cap_3 = Vn*Rfe./(Rfe+Zcl+Zlr);
Ig = Vs/(Rs+Rl);
I2=Ig.*Zlgr.*(Zl+Zdne)./(Zdfe.*Zdne-Zl.^2);
Vne_ind_3=Rne*I2;
I1=Ig.*Zlgr.*(Zl+Zdfe)./(Zdfe.*Zdne-Zl.^2);
Vfe_ind_3=Rfe*I1;

% Ll = 9.04e-9;
Ll = 9.04e-9;
Zlr = j*w*Lr/2;
Zcr = -j./(w*Cr);
Zll = j*w*Ll;
Zcgr = -j./(w*Cgr);
Zcg = -j./(w*Cg);
Zcl = -j./(2*w*Cl);
Zl = Zcr.*Zll./(Zcr+Zll);
Zdne = Zcl+Zlr+Rne+Zl;
Zdfe = Zcl+Zlr+Rfe+Zl;
Zlgr = j*w*Lgr/2;
Zne = Zcl+Zlr+Rne;
Zfe = Zcl+Zlr+Rfe;

Vin = Vs*Rl/(Rl+Rs);
Zeq = Zne.*Zfe.*Zl./(Zfe.*Zl+Zne.*Zl+Zne.*Zfe);
Vn = Vin*Zeq./(Zeq+Zcgr);
Vne_cap_4 = Vn*Rne./(Rne+Zcl+Zlr);
Vfe_cap_4 = Vn*Rfe./(Rfe+Zcl+Zlr);
```

```
Ig = Vs/(Rs+Rl);
I2=Ig.*Zlgr.*(Zl+Zdne)./(Zdfe.*Zdne-Zl.^2);
Vne_ind_4=Rne*I2;
I1=Ig.*Zlgr.*(Zl+Zdfe)./(Zdfe.*Zdne-Zl.^2);
Vfe_ind_4=Rfe*I1;

%%%%%%%%%%%%%%%%%%%%%%%%%%%%%%%%%%%% Varying values of C_l %%%%%%%%%%%%%%%%%%%%%%%%%%
% Cl=0.3e-12
Ll = 3.04e-9;
Cl = 0.3e-12;
Zlr = j*w*Lr/2;
Zcr = -j./(w*Cr);
Zll = j*w*Ll;
Zcgr = -j./(w*Cgr);
Zcg = -j./(w*Cg);
Zcl = -j./(2*w*Cl);
Zl = Zcr.*Zll./(Zcr+Zll);
Zdne = Zcl+Zlr+Rne+Zl;
Zdfe = Zcl+Zlr+Rfe+Zl;
Zlgr = j*w*Lgr/2;
Zne = Zcl+Zlr+Rne;
Zfe = Zcl+Zlr+Rfe;

Vin = Vs*Rl/(Rl+Rs);
Zeq = Zne.*Zfe.*Zl./(Zfe.*Zl+Zne.*Zl+Zne.*Zfe);
Vn = Vin*Zeq./(Zeq+Zcgr);
Vne_cap_5 = Vn*Rne./(Rne+Zcl+Zlr);
Vfe_cap_5 = Vn*Rfe./(Rfe+Zcl+Zlr);
Ig = Vs/(Rs+Rl);
I2=Ig.*Zlgr.*(Zl+Zdne)./(Zdfe.*Zdne-Zl.^2);
Vne_ind_5=Rne*I2;
I1=Ig.*Zlgr.*(Zl+Zdfe)./(Zdfe.*Zdne-Zl.^2);
Vfe_ind_5=Rfe*I1;

% Cl = 0.5e-12;
Cl = 0.5e-12;
Zlr = j*w*Lr/2;
Zcr = -j./(w*Cr);
Zll = j*w*Ll;
Zcgr = -j./(w*Cgr);
Zcg = -j./(w*Cg);
Zcl = -j./(2*w*Cl);
Zl = Zcr.*Zll./(Zcr+Zll);
Zdne = Zcl+Zlr+Rne+Zl;
Zdfe = Zcl+Zlr+Rfe+Zl;
Zlgr = j*w*Lgr/2;
Zne = Zcl+Zlr+Rne;
Zfe = Zcl+Zlr+Rfe;

Vin = Vs*Rl/(Rl+Rs);
Zeq = Zne.*Zfe.*Zl./(Zfe.*Zl+Zne.*Zl+Zne.*Zfe);
Vn = Vin*Zeq./(Zeq+Zcgr);
Vne_cap_6 = Vn*Rne./(Rne+Zcl+Zlr);
Vfe_cap_6 = Vn*Rfe./(Rfe+Zcl+Zlr);
Ig = Vs/(Rs+Rl);
I2=Ig.*Zlgr.*(Zl+Zdne)./(Zdfe.*Zdne-Zl.^2);
Vne_ind_6=Rne*I2;
I1=Ig.*Zlgr.*(Zl+Zdfe)./(Zdfe.*Zdne-Zl.^2);
Vfe_ind_6=Rfe*I1;

% Cl = 0.7e-12;
Cl = 0.7e-12;
Zlr = j*w*Lr/2;
Zcr = -j./(w*Cr);
Zll = j*w*Ll;
Zcgr = -j./(w*Cgr);
```

```
Zcg = -j./(w*Cg);
Zcl = -j./(2*w*Cl);
Zl = Zcr.*Zll./(Zcr+Zll);
Zdne = Zcl+Zlr+Rne+Zl;
Zdfe = Zcl+Zlr+Rfe+Zl;
Zlgr = j*w*Lgr/2;
Zne = Zcl+Zlr+Rne;
Zfe = Zcl+Zlr+Rfe;

Vin = Vs*Rl/(Rl+Rs);
Zeq = Zne.*Zfe.*Zl./(Zfe.*Zl+Zne.*Zl+Zne.*Zfe);
Vn = Vin*Zeq./(Zeq+Zcgr);
Vne_cap_7 = Vn*Rne./(Rne+Zcl+Zlr);
Vfe_cap_7 = Vn*Rfe./(Rfe+Zcl+Zlr);
Ig = Vs/(Rs+Rl);
I2=Ig.*Zlgr.*(Zl+Zdne)./(Zdfe.*Zdne-Zl.^2);
Vne_ind_7=Rne*I2;
I1=Ig.*Zlgr.*(Zl+Zdfe)./(Zdfe.*Zdne-Zl.^2);
Vfe_ind_7=Rfe*I1;

% Cl = 0.9e-12;
Cl = 0.9e-12;
Zlr = j*w*Lr/2;
Zcr = -j./(w*Cr);
Zll = j*w*Ll;
Zcgr = -j./(w*Cgr);
Zcg = -j./(w*Cg);
Zcl = -j./(2*w*Cl);
Zl = Zcr.*Zll./(Zcr+Zll);
Zdne = Zcl+Zlr+Rne+Zl;
Zdfe = Zcl+Zlr+Rfe+Zl;
Zlgr = j*w*Lgr/2;
Zne = Zcl+Zlr+Rne;
Zfe = Zcl+Zlr+Rfe;

Vin = Vs*Rl/(Rl+Rs);
Zeq = Zne.*Zfe.*Zl./(Zfe.*Zl+Zne.*Zl+Zne.*Zfe);
Vn = Vin*Zeq./(Zeq+Zcgr);
Vne_cap_8 = Vn*Rne./(Rne+Zcl+Zlr);
Vfe_cap_8 = Vn*Rfe./(Rfe+Zcl+Zlr);
Ig = Vs/(Rs+Rl);
I2=Ig.*Zlgr.*(Zl+Zdne)./(Zdfe.*Zdne-Zl.^2);
Vne_ind_8=Rne*I2;
I1=Ig.*Zlgr.*(Zl+Zdfe)./(Zdfe.*Zdne-Zl.^2);
Vfe_ind_8=Rfe*I1;

Vne_total_1 = Vne_cap_1 + Vne_ind_1;
Vne_total_2 = Vne_cap_2 + Vne_ind_2;
Vne_total_3 = Vne_cap_3 + Vne_ind_3;
Vne_total_4 = Vne_cap_4 + Vne_ind_4;

Vne_total_5 = Vne_cap_5 + Vne_ind_5;
Vne_total_6 = Vne_cap_6 + Vne_ind_6;
Vne_total_7 = Vne_cap_7 + Vne_ind_7;
Vne_total_8 = Vne_cap_8 + Vne_ind_8;

Vfe_total_1 = Vfe_cap_1 + Vfe_ind_1;
Vfe_total_2 = Vfe_cap_2 + Vfe_ind_2;
Vfe_total_3 = Vfe_cap_3 + Vfe_ind_3;
Vfe_total_4 = Vfe_cap_4 + Vfe_ind_4;

Vfe_total_5 = Vfe_cap_5 + Vfe_ind_5;
Vfe_total_6 = Vfe_cap_6 + Vfe_ind_6;
Vfe_total_7 = Vfe_cap_7 + Vfe_ind_7;
Vfe_total_8 = Vfe_cap_8 + Vfe_ind_8;
```

```
figure
p1=plot(f./1e9,20*log10(abs(Vne_cap_1)),'k',f./1e9,20*log10(abs(Vne_cap_2)),'--k',f./1e9,20*log10
(abs(Vne_cap_3)),'-^k',f./1e9,20*log10(abs(Vne_cap_4)),'-Ok',f./1e9,20*log10(abs(Vne_ind_1)),'.k',
f./1e9,20*log10(abs(Vne_ind_2)),'*k',f./1e9,20*log10(abs(Vne_ind_3)),'-*k',f./1e9,20*log10
(abs(Vne_ind_4)),'-.k')
legend('V_{ne}^{CAP} for L_L = 3.04 nH','V_{ne}^{CAP} for L_L
= 5.04 nH','V_{ne}^{CAP} for L_L = 7.04 nH','V_{ne}^{CAP} for L_L =
9.04 nH','V_{ne}^{IND} for L_L = 3.04 nH','V_{ne}^{IND} for L_L =
5.04 nH','V_{ne}^{IND} for L_L = 7.04 nH','V_{ne}^{IND} for L_L =
9.04 nH') set(p1,'Linewidth',1.5) xlabel('f (GHz)') ylabel('|V|
(dB)') title('Effect of L_L on  V_{ne}Cap  and  V_{ne}Ind for Z_L =
2 Ohms') axis([0.5 3 -200 0])

figure
p2=plot(f./1e9,20*log10(abs(Vne_total_1)),'k',f./1e9,20*log10(abs(Vne_total_2)),'--k',f./1e9,
20*log10(abs(Vne_total_3)),'-^k',f./1e9,20*log10(abs(Vne_total_4)),'-Ok')
legend('V_{ne}^{TOT} for L_L = 3.04 nH','V_{ne}^{TOT} for L_L = 5.04 nH','V_{ne}^{TOT} for
L_L = 7.04 nH','V_{ne}^{TOT} for L_L = 9.04 nH')
set(p2,'Linewidth',1.5)
xlabel('f (GHz)')
ylabel('|V| (dB)')
title('Effect of L_L on  V_{ne}Total for Z_L = 2 Ohms')
axis([0.5 3 -200 0])

figure
p3=plot(f./1e9,20*log10(abs(Vne_cap_5)),'k',f./1e9,20*log10(abs(Vne_cap_6)),'--k',f./1e9,20*log10
(abs(Vne_cap_7)),'-^k',f./1e9,20*log10(abs(Vne_cap_8)),'-Ok',f./1e9,20*log10(abs(Vne_ind_5)),'.k',
f./1e9,20*log10(abs(Vne_ind_6)),'*k',f./1e9,20*log10(abs(Vne_ind_7)),'-*k',f./1e9,20*log10
(abs(Vne_ind_8)),'-.k')
legend('V_{ne}^{CAP} for C_L = 0.3 pF','V_{ne}^{CAP} for C_L =
0.5 pF','V_{ne}^{CAP} for C_L = 0.7 pF','V_{ne}^{CAP} for C_L = 0.9
pF','V_{ne}^{IND} for C_L = 0.3 pF','V_{ne}^{IND} for C_L = 0.5
pF','V_{ne}^{IND} for C_L = 0.7 pF','V_{ne}^{IND} for C_L = 0.9 pF')
set(p3,'Linewidth',1.5) xlabel('f (GHz)') ylabel('|V| (dB)')
title('Effect of C_L on  V_{ne}Cap  and  V_{ne}Ind for Z_L = 2
Ohms') axis([0.5 3 -200 0])

figure
p4=plot(f./1e9,20*log10(abs(Vne_total_5)),'k',f./1e9,20*log10(abs(Vne_total_6)),'--k',f./1e9,
20*log10(abs(Vne_total_7)),'-^k',f./1e9,20*log10(abs(Vne_total_8)),'-Ok')
legend('V_{ne}^{TOT} for C_L = 0.3 pF','V_{ne}^{TOT} for C_L = 0.5 pF','V_{ne}^{TOT} for
C_L = 0.7 pF','V_{ne}^{TOT} for C_L = 0.9 pF')
set(p4,'Linewidth',1.5)
xlabel('f (GHz)')
ylabel('|V| (dB)')
title('Effect of C_L on  V_{ne}Total for Z_L = 2 Ohms')
axis([0.5 3 -200 0])

figure
p5=plot(f./1e9,20*log10(abs(Vfe_cap_1)),'k',f./1e9,20*log10(abs(Vfe_ind_1)),'k',f./1e9,20*log10
(abs(Vfe_cap_2)),'--k',f./1e9,20*log10(abs(Vfe_ind_2)),'--k',f./1e9,20*log10(abs(Vfe_cap_3)),'-^k',
f./1e9,20*log10(abs(Vfe_ind_3)),'-^k',f./1e9,20*log10(abs(Vfe_cap_4)),'-Ok',f./1e9,20*log10
(abs(Vfe_ind_4)),'-Ok')
legend('V_{fe}^{CAP} for L_L = 3.04 nH','V_{fe}^{IND} for L_L =
3.04 nH','V_{fe}^{CAP} for L_L = 5.04 nH','V_{fe}^{IND} for L_L =
5.04 nH','V_{fe}^{CAP} for L_L = 7.04 nH','V_{fe}^{IND} for L_L =
7.04 nH','V_{fe}^{CAP} for L_L = 9.04 nH','V_{fe}^{IND} for L_L = 9.04 nH')
set(p5,'Linewidth',1.5)
xlabel('f (GHz)')
ylabel('|V| (dB)')
title('Effect of L_L on  V_{fe}Cap  and  V_{fe}Ind for Z_L = 2 Ohms')
axis([0.5 3 -200 0])

figure
p6=plot(f./1e9,20*log10(abs(Vfe_total_1)),'k',f./1e9,20*log10(abs(Vfe_total_2)),'--k',f./1e9,
20*log10(abs(Vfe_total_3)),'-^k',f./1e9,20*log10(abs(Vfe_total_4)),'-Ok')
```

```
legend('V_{fe}^{TOT} for L_L = 3.04 nH','V_{fe}^{TOT} for L_L = 5.04 nH','V_{fe}^{TOT} for
L_L = 7.04 nH','V_{fe}^{TOT} for L_L = 9.04 nH')
set(p6,'Linewidth',1.5)
xlabel('f (GHz)')
ylabel('|V| (dB)')
title('Effect of L_L on  V_{fe}Total for Z_L = 2 Ohms')
axis([0.5 3 -200 0])

figure
p7=plot(f./1e9,20*log10(abs(Vfe_cap_5)),'k',f./1e9,20*log10(abs(Vfe_ind_5)),'k',f./1e9,20*log10
(abs(Vfe_cap_6)),'--k',f./1e9,20*log10(abs(Vfe_ind_6)),'--k',f./1e9,20*log10(abs(Vfe_cap_7)),'-^k',
f./1e9,20*log10(abs(Vfe_ind_7)),'-^k',f./1e9,20*log10(abs(Vfe_cap_8)),'-Ok',f./1e9,20*log10
(abs(Vfe_ind_8)),'-Ok')
legend('V_{fe}^{CAP} for C_L = 0.3 pF','V_{fe}^{IND} for C_L =
0.3 pF','V_{fe}^{CAP} for C_L = 0.5 pF','V_{fe}^{IND} for C_L =
0.5 pF','V_{fe}^{CAP} for C_L = 0.7 pF','V_{fe}^{IND} for C_L =
0.7 pF','V_{fe}^{CAP} for C_L = 0.9 pF','V_{fe}^{IND} for C_L = 0.9 pF')
set(p7,'Linewidth',1.5)
xlabel('f (GHz)')
ylabel('|V| (dB)')
title('Effect of C_L on  V_{fe}Cap  and  V_{fe}Ind for Z_L = 2 Ohms')
axis([0.5 3 -200 0])

figure
p8=plot(f./1e9,20*log10(abs(Vfe_total_5)),'k',f./1e9,20*log10(abs(Vfe_total_6)),'--k',f./1e9,
20*log10(abs(Vfe_total_7)),'-^k',f./1e9,20*log10(abs(Vfe_total_8)),'-Ok')
legend('V_{fe}^{TOT} for C_L = 0.3 pF','V_{fe}^{TOT} for C_L = 0.5 pF','V_{fe}^{TOT} for
C_L = 0.7 pF','V_{fe}^{TOT} for C_L = 0.9 pF')
set(p8,'Linewidth',1.5)
xlabel('f (GHz)')
ylabel('|V| (dB)')
title('Effect of C_L on  V_{fe}Total for Z_L = 2 Ohms')
axis([0.5 3 -200 0])
```

APPENDIX C. MATLAB CODE : RH-CSRR COUPLING

The following file

`RH_CSRR_Coupling.m`.

was used to determine the near-end and far-end capacitive, inductive and total coupling for RH- and CSRR-TL unit cell for different values of load terminations.

```
%%%%%%%%%%%%%%%%%%%%%%%%%%%%%%%% RH_CSRR_COUPLING FILE %%%%%%%%%%%%%%%%%%%%%%%%%%%%%%%%
%%%%%%%%%%%%%%%%%%%%%%%%%%%%%%%%%%%%%%%%%%%%%%%%%%%%%%%%%%%%%%%%%%%%%%%%%%%%%%%%%%%%%%%
clc
clear all
close all

f = 100e6:10e6:3e9;
w=2*pi*f;
Vs = 1;
Rs = 50;
Cc=19.58e-12;
Cg = 1.968e-12;
Cgr = .06786e-12;
Lr = 4.96e-9;
Rl = 20;
Rne = 200;
Rfe = 200;
Cr = 4.01e-12;
Ll = 3.22e-9;
Cl = 1.27e-12;
Lgr = .11036e-9;

Zlr = j*w*Lr/2;
Zcr = -j./(w*Cr);
Zll = j*w*Ll;
Zcgr = -j./(w*Cgr);
Zcg = -j./(w*Cg);
Zcl = -j./(2*w*Cl);
Zl = ((Zcr.*Zll)./(Zcr+Zll))-j./(w*Cc);
Zdne = Zcl+Zlr+Rne+Zl;
Zdfe = Zcl+Zlr+Rfe+Zl;
Zlgr = j*w*Lgr/2;
Zne = Zcl+Zlr+Rne;
Zfe = Zcl+Zlr+Rfe;

%%%%%%%%%%%%%%%%%%%%%% Capacitive Coupling%%%%%%%%%%%%%%%%%%%%%%%%%%
figure
Vin = Vs*Rl/(Rl+Rs);
Zeq = Zne.*Zfe.*Zl./(Zfe.*Zl+Zne.*Zl+Zne.*Zfe);
Vn = Vin*Zeq./(Zeq+Zcgr);
Vne_cap = Vn*Rne./(Rne+Zcl+Zlr);
Vfe_cap = Vn*Rfe./(Rfe+Zcl+Zlr);
plot(f,20*log10(abs(Vne_cap)),'.',f,20*log10(abs(Vfe_cap)),'-')
xlabel('f (Hz)')
ylabel('|V| (dB)')
legend('V_{ne}','V_{fe}')
title('Capacitive Coupling')
axis([0 2e9 -110 -30])
grid on

%%%%%%%%%%%%%%%%%%%%%%Inductive Coupling%%%%%%%%%%%%%%%%%%%%%%%%%%
figure
```

```
Ig = Vs/(Rs+Rl);
I2=Ig.*Zlgr.*(Zl+Zdne)./(Zdfe.*Zdne-Zl.^2);
Vne_ind=Rne*I2;
I1=Ig.*Zlgr.*(Zl+Zdfe)./(Zdfe.*Zdne-Zl.^2);
Vfe_ind=Rfe*I1;
plot(f,20*log10(abs(Vne_ind)),'.',f,20*log10(abs(Vfe_ind)),'-')
xlabel('f (Hz)')
ylabel('|V| (dB)')
legend('V_{ne}','V_{fe}')
title('Inductive Coupling')
axis([0 2e9 -110 -30])
grid on

%%%%%%%%%%%%%%%%%Near-end Total Coupling%%%%%%%%%%%%%%%%%%%%%%%%%%%%
figure
Vne=Vne_cap+Vne_ind;
plot(f,20*log10(abs(Vne)),'.k',f,20*log10(abs(Vne_ind)),'--k', ...
    f,20*log10(abs(Vne_cap)),'-k')
xlabel('f (Hz)')
ylabel('|V_{NE}| (dB)')
title('Near-End Total Coupling')
legend('V_{ne}^{TOT}','V_{ne}^{IND}','V_{ne}^{CAP}')
axis([0 2e9 -110 -30])
grid on

%%%%%%%%%%%%%%%%%%%%Far-end Total Coupling%%%%%%%%%%%%%%%%%%%%%%%%%%%%
figure
Vfe=Vfe_cap+Vfe_ind;
plot(f,20*log10(abs(Vfe)),'.',f,20*log10(abs(Vfe_ind)),'--', ...
    f,20*log10(abs(Vfe_cap)),'-')
xlabel('f (Hz)')
ylabel('|V| (dB)')
title('Far-End Total Coupling')
legend('V_{fe}^{TOT}','V_{fe}^{IND}','V_{fe}^{CAP}')
axis([0 2e9 -110 -30])
grid on
```